PHOTONICS Research

Phase segregation in inorganic mixed-halide perovskites: from phenomena to mechanisms

Yutao Wang,[1] Xavier Quintana,[2] Jiyun Kim,[1] Xinwei Guan,[1] Long Hu,[1] Chun-Ho Lin,[1] Brendon Tyler Jones,[2] Weijian Chen,[3] Xiaoming Wen,[3] Hanwei Gao,[2,4] and Tom Wu[1,5]

[1]School of Materials Science and Engineering and Advanced Materials and Manufacturing Futures Institute, University of New South Wales (UNSW), Sydney, NSW 2052, Australia
[2]Department of Physics, Florida State University, Tallahassee, Florida 32306, USA
[3]Centre for Translational Atomaterials, Swinburne University of Technology, Hawthorn, VIC 3122, Australia
[4]e-mail: hanwei.gao@fsu.edu
[5]e-mail: tom.wu@unsw.edu.au

Received 9 July 2020; revised 19 August 2020; accepted 1 September 2020; posted 2 September 2020 (Doc. ID 402411); published 30 October 2020

Halide perovskites, such as methylammonium lead halide perovskites ($MAPbX_3$, X = I, Br, and Cl), are emerging as promising candidates for a wide range of optoelectronic applications, including solar cells, light-emitting diodes, and photodetectors, due to their superior optoelectronic properties. All-inorganic lead halide perovskites $CsPbX_3$ are attracting a lot of attention because replacing the organic cations with Cs^+ enhances the stability, and its halide-mixing derivatives offer broad bandgap tunability covering nearly the entire visible spectrum. However, there is evidence suggesting that the optical properties of mixed-halide perovskites are influenced by phase segregation under external stimuli, especially illumination, which may negatively impact the performance of optoelectronic devices. It is reported that the mixed-halide perovskites in forms of thin films and nanocrystals are segregated into a low-bandgap I-rich phase and a high-bandgap Br-rich phase. Herein, we present a critical review on the synthesis and basic properties of all-inorganic perovskites, phase-segregation phenomena, plausible mechanisms, and methods to mitigate phase segregation, providing insights on advancing mixed-halide perovskite optoelectronics with reliable performance.

https://doi.org/10.1364/PRJ.402411

1. INTRODUCTION

The research of functional materials, especially semiconductors, is critical for advancing a wide range of technologies for electronics, energy conversion, sensing, and so on. Recently, the metal halide perovskites have aroused significant interests due to the auspicious performance, lower cost, and convenient synthesis methods. Perovskites are becoming the most promising photoelectronic materials and have been applied in diverse applications, including solar cells [1–7], lasers [8–11], light-emitting diodes (LEDs) [12–16], and photodetectors [17–25]. Owing to excellent optoelectronic properties, such as strong optical absorption, relatively low trap state density, high carrier mobility, and long diffusion length [26–33], the power conversion efficiency (PCE) of perovskite solar cells has rapidly caught up with silicon solar cells in only a few years of development. The first perovskite solar cell was fabricated by Miyasaka and coworkers in 2009, giving out the PCE of 3.8%; the efficiency has been boosted to around 25% these years [2,34]. Similarly, the first perovskite LED was fabricated by Tan *et al.* and exhibited an external quantum efficiency (EQE) of 0.76%. Red and green LEDs have been reported to exhibit EQEs of over 20% and 25%, respectively, while blue LEDs have struggled to reach the 15% mark [12,35].

Halide perovskites take the chemical formation of ABX_3 [36], where the A site is a cation situated in the void between eight BX_6 octahedra, the B site is occupied by a cation, usually a divalent metal such as Pb^{2+} or Sn^{2+}, and the X site contains the monovalent halide ion(s) I^-, Br^-, and/or Cl^- [37]. The monovalent A cation can be organic elements such as methylammonium (MA^+) and formamidinium (FA^+) or inorganic elements such as Cs^+ or their mixtures. Compositional engineering involving the mixing of cations or anions is a widely adaptable approach toward tunable bandgap and enhanced stability [38,39]. Furthermore, mixing Cl^-, Br^-, and I^- can effectively tune the perovskite bandgap in the range between 1.75 eV ($CsPbI_3$) and 2.4 eV ($CsPbCl_3$), which is favorable for optoelectronic applications [40–42].

This perspective focuses on inorganic mixed-halide perovskites because of their outstanding optoelectronic properties and high device stability [43]. Perovskite materials are exhibiting severe stability problems because of polymorphic transition, hydration, decomposition, and oxidation [44]. Compared to the organic–inorganic hybrid halide perovskites with A-site cations like MA^+ or FA^+, all-inorganic perovskites based on Cs^+ cation exclude the degradation caused by the hydration of organic cations and possess superior stability against moisture, heat, illumination, and electron beams [43].

$CsPbI_3$ perovskite is metastable in the optoelectronically favorable "black phase" at high temperatures, but it spontaneously transitions to a "yellow" nonperovskite phase at room temperature [45,46]. Mixing halogen ions can mitigate this problem and stabilize the perovskite phase. The Goldschmidt tolerance factor (T.F.) relates a crystal stability to the distortion of its lattice and should be equal to 1 to obtain the ideal perovskite structure, but distorted lattices can still be stabilized when $0.8 < \text{T.F.} < 1.1$ [47], which allows for the high flexibility of compositional engineering in halide perovskites. The T.F. of $CsPbI_3$ perovskite is as low as 0.8, resulting in the structural instability and triggering the transformation of "black" perovskite to "yellow" nonperovskite polymorphs at room temperature [45]. However, the optical properties of mixed-halide perovskites are not as robust as initially assumed. In particular, phase segregation in mixed-halide perovskites $MAPb(I_{1-x}Br_x)_3$ was discovered by Hoke *et al.* in 2015 [48]. The effect manifested as red shifts of both absorption and emission peaks toward I-rich compositions. It was hypothesized that under continuous optical irradiation, mixed-halide perovskites undergo reversible halide phase segregation into I-rich and Br-rich domains. Light-induced halide phase segregation has been confirmed through optical and structural measurements in a plethora of hybrid and all-inorganic perovskite compositions [49–63]. This ubiquitous phenomenon, although contradictory sometimes, has been reported in thin films and nanocrystals (NCs). To date, some reviews have discussed the phase segregation in organic–inorganic hybrid perovskites [64–66]. This review aims to address the discrepancies between phase-segregation mechanisms and provide insight into the current state of inorganic mixed-halide perovskite.

The importance of phase segregation in perovskites and its influence on photovoltaic device performance have been recognized by the community [53,56–58,67]. It was proposed that the often-observed reductions of open-circuit voltage (V_{OC}) and short-circuit current density (J_{SC}) of mixed-halide perovskite solar cells upon light illumination could be correlated with phase segregation [67]. Light-induced halide migration can lead to anion accumulation at the interfaces between hybrid perovskite and charge extraction layers, creating injection barriers and jeopardizing device performance [58,68]. Further investigation into the mechanisms governing phase segregation should be taken into consideration in order to retain the reliable operation of perovskite devices under strong light illumination or other environmental stimuli.

In this review, we will first discuss the synthesis of inorganic halide perovskites in both thin film and NC forms that is the foundation of investigating the optical and basic properties of perovskites. Then we review the recent experimental observations of phase segregation in comparison to the widely reported phenomena in the hybrid counterparts. Finally, the proposed mechanisms of phase segregation in all-inorganic mixed-halide perovskites are discussed along with the mitigation methods for achieving reliable device operation.

2. SYNTHESIS AND BASIC PROPERTIES OF INORGANIC HALIDE PEROVSKITES

A. Synthesis Methods

Rational synthesis is the foundation of investigating the properties of inorganic perovskites and evaluating their potential for device applications. The subtle differences in synthesis often explain the discrepancies on the physical properties of the samples, including phase segregation and other reported phenomena. To date, the synthesis methods involved in the reports on phase segregation in inorganic perovskite thin films are majorly solution-processed spin coating and vapor-phase thermal evaporation, while colloidal solution-based methods have been widely used for producing NCs.

One-step spin coating for perovskite film deposition was introduced first by Miyasaka *et al.* in the fabrication of hybrid perovskite solar cells [2]. After that, many modified one- and two-step methods for perovskite synthesis were carried out to improve the crystallinity and morphological properties of perovskite absorbers. The deposition of high-quality all-inorganic perovskite thin films is challenging because of the solubility limitations of some Cs-salts, like CsBr, in the commonly used solvents [i.e., dimethylformamide (DMF) and dimethyl sulfoxide (DMSO)]. One-step deposition of all-inorganic $CsPbI_3Br$ was reported by Moore *et al.* [69], and the perovskite film was thin (150 nm) because of the limitation of solubility (0.4 mol/L in DMF). Soon after this work, Park *et al.* optimized the annealing temperature to control the crystallization process of all-inorganic $CsPbI_2Br$ and observed that a film's intrinsic phase stability was improved by annealing at elevated temperatures [70].

Since two or more halide precursors are included in the synthesis of inorganic mixed-halide perovskite films, the solvent needs to be carefully selected to improve the solubility. The utilization of a cosolvent, like the addition of DMSO in DMF with optimized ratios (1:4), was reported by many groups to improve the solubility of precursors up to 1.2 mol/L [69,71,72]. Particularly, the gradual release of DMSO during the annealing of films may promote the crystallization and stabilization of PbI-intermediate phase formation. It was noted that the DMSO inclusion should not be higher than 40% because an excessive DMSO ratio causes smaller grain sizes and formation of pinholes. The composition of the resulting film using one-step processing is heavily dictated by the evaporation of the solvent, which can result in inhomogeneity. The choice of solvent has been shown to affect halide distribution as well. Yoon *et al.* showed how lead complexation in the precursor solution leads to preferential complexation with Br^- ions compared to I^-. The group found that the complexation constant for the tetrabromide complex was 3.5 times greater than that of tetraiodide using DMF [73]. With proper solvent engineering, inorganic perovskite thin

films with the thickness of hundreds of nm and excellent uniformity were achieved.

Two-step spin-coating deposition was another strategy for the thin film deposition introduced by Im *et al.* [74], which was later adopted by many other groups to fabricate perovskite films. For example, Burschka *et al.* reported a two-step spin-coating method coating a high concentration PbI_2 solution layer onto TiO_2 and then exposed it to CH_3NH_2I solution in 2-propanol and successfully deposited large-area perovskite films [71]. Jeon *et al.* demonstrated that the utilization of a mixed solvent (γ-butyrolactone/DMSO) followed by toluene drop-casting resulted in extremely homogeneous and smooth hybrid mixed-halide perovskite films [75]. In the case of inorganic perovskite films, Lou *et al.* reported a supersaturated-recrystallization method involving the incorporation of NH_4Br into the saturated solution of $PbBr_2$ and CsBr, which yielded a film with a photoluminescence quantum yield (PLQY) of 40.8% [76]. Generally, the major motivation of using a two-step deposition method is to address the low solubility issue of CsBr in the commonly utilized organic solvents and to suppress pinholes, resulting in better film qualities. Although the two-step spin-coating process has not been reported for the investigation of phase segregation, it is a factor to consider for the preparation of stable inorganic perovskite films.

Perovskite thin films deposited under vacuum, like thermal evaporation, presented better control of thicknesses and morphology compared to solution-based coating processes. An additional benefit is that deposition under vacuum is a well-established technique in photovoltaic/LED manufacturing, making it compatible with the existing infrastructure. Gaonkar *et al.* reported a commercially viable approach to fabricate all-inorganic mixed-halide perovskite using vacuum deposition. The resulting films demonstrated exceptional thermal stability, with no loss in performance after 72 h at 200°C. The increased performance can be partially attributed to the increased control over the precursors which can yield a stoichiometrically correct perovskite [77]. In another representative work, Ma *et al.* reported the deposition of $CsPbIBr_2$ thin film through dual-source thermal evaporation with the equimolar quantities of CsI and $PbBr_2$, characterized by X-ray photoelectron spectroscopy (XPS) [78]. The photoluminescence (PL) characterization showed a stabilized PL peak during the illumination process, indicating the absence of halide phase segregation in this perovskite film. Lin *et al.* reported vacuum-deposited inorganic perovskite films with suppressed hysteresis and ion transport in the solar cell active layer [79]. They demonstrated that the $CsPbI_2Br$ thin films with good morphology could be achieved by the stoichiometric control of CsBr and PbI_2 through cosublimation under a high vacuum. The as-synthesized films possess small crystalline grain sizes down to 100 nm and increase to 3 μm after subsequent annealing. The device based on this vacuum-deposited $CsPbI_2Br$ film exhibited negligible hysteresis, indicating suppressed ion migration in the film. Moreover, vacuum deposition introduces new variables that affect the morphology of the film, such as layer thickness and substrate temperature, which will be discussed in the section of mitigation methods.

Perovskite NCs were also chosen for the investigation of phase segregation because of the intrinsically small crystal size and limited diffusion length, resulting in suppressed halide segregation [16,52,61,63]. The first inorganic perovskite NC colloidal solutions were introduced by Loredana *et al.*, together with the NC-based light-emitting devices which featured bright, stable, spectrally narrow, and broadly tunable PL [40]. The NCs were fabricated via the injection of the Cs-oleate solution to the PbX_2 solution with the complete sublimation of the PbX_2 salt after the injection of oleylamine and oleic acid. The NCs were further treated with isolation and purification and then dispersed in toluene or hexane to form long-term colloidally stable solutions. This method allowed Gualdrón-Reyes *et al.* to easily alter the NC size and develop a relationship between NC size and phase segregation [63]. Later on, Yang *et al.* reported a fabrication strategy assisted by a layer-by-layer spin coating for high-quality $CsPbI_2Br$ perovskite NC film [80]. Highly smooth and pinhole-free NC films were obtained after annealing at 260°C, and the spacing between NCs can be adjusted by removing the insulating ligand through 2-propanol washing. One motivation to fabricate perovskite NCs, including the mixed-halide ones, is to achieve good stability under ambient conditions. Understanding the chemistry and kinetics of the colloidal solution helps improve the properties of perovskite NCs films, including the suppression of halide migration and segregation. Fabricating perovskite NCs is an excellent method to mitigate phase segregation, yet the limited diffusion length makes charge extraction difficult, so it may be an impractical approach for solar cell implementation.

The choice of substrate has been shown to affect the crystallization behavior of the perovskite film. Hu *et al.* reported that the application of a nonwetting hole transport layer improved device performance due to the increase in grain size [57]. A wetting surface reduces the contact angle, and therefore the Gibbs free energy, promoting the formation of small, dense nuclei. Conversely, a nonwetting surface suppresses nucleation and leads to the formation of larger grains, a potential solution to suppressing the ion accumulation at the grain boundaries [57]. Furthermore, the porosity of the substrate was shown to alter the macrostructure as well. It was reported that increasing the thickness of the scaffolding reduces the PL lifetime and blue shifts the emission as a result of the fully mesostructured film [81].

The impact of synthesis techniques on phase segregation has not yet been clearly studied, but the impact on morphology differs from each synthesis technique and can be used to correlate phase-segregation behaviors with the selected procedures. One-step deposition often yields films with more pinholes which have been reported to reduce the shunt resistance in perovskite solar cells [82]. This may have the consequence of increasing the phase-segregation rate due to the larger grain boundary density, where segregated halide ions have been reported to accumulate. Additionally, *ab initio* molecular dynamics simulations suggest defects may provide low energy pathways for ions to travel and facilitate phase segregation [54]. Two-step deposition procedures have the potential to synthesize smoother, pinhole free films through the utilization of the cosolvent. Both techniques, however, rely on spin-coating and a precursor solvent which can introduce inhomogeneity in the form of a breakup or crystal alignment [83]. Proper

revolution speed and the choice of solvent are crucial in mitigating the formation of grain boundaries and suppressing phase segregation.

In the case of vacuum deposition, the highly mobile precursor molecules arrange themselves in a diffuse and stable configuration that leads to high density and stability. The random orientation of deposited molecules was shown to be thermodynamically stable by Yokoyama *et al.* [84]. Although this random orientation exhibits high thermal stability, it also increases the density of grain boundaries and further facilitates phase segregation. Layer-by-layer deposition introduces the halide imbalance at the layer boundaries; this acts as a driving force for phase segregation [54] and can lead to the presence of an unreacted layer if the precursors do not diffuse enough into the film upon contact.

B. Optical Properties of Inorganic Perovskites

All-inorganic perovskites often possess multiple structural phases, and phase transitions can be triggered by external stimuli. The cubic phase $CsPbI_3$ (α-$CsPbI_3$) has a bandgap of 1.73 eV, making it a promising candidate as the absorber layer in perovskite solar cells [85]. However, the α-$CsPbI_3$ can only be obtained above 315°C and is only metastable at room temperature. The partial substitution of I^- by Br^- has been demonstrated to lower the phase transition temperature and stabilize the cubic phase of $CsPbI_3$ at the cost of an increased bandgap.

$CsPbI_3$ transforms to tetragonal (β-$CsPbI_3$) and orthorhombic (γ-$CsPbI_3$) at a higher temperature of 281°C and 184°C, respectively [Fig. 1(a)] [86–90]. Furthermore, the γ-$CsPbI_3$ phase subsequently transforms into the nonperovskite δ-$CsPbI_3$ phase after being exposed to the ambient air, and it can be reversed back to the cubic phase after being heated to above 315°C [45]. The yellow δ-$CsPbI_3$ phase is detrimental to the photovoltaic applications because of its large bandgap (2.83 eV) and poor electronic transport. As a result, it is critical to develop synthesis and additive strategies to maintain the cubic α-$CsPbI_3$ phase, which is a hot topic for inorganic perovskite research [91,92]. For other halide compositions such as $CsPbIBr_3$ and $CsPbCl_3$, the perovskite structures undergo a phase transition from cubic to tetragonal at 130°C and 47°C, from tetragonal to orthorhombic at 88°C and 42°C, respectively [69,93]. Furthermore, mixing halide ions in perovskites allows for the ability to tune the bandgap over the entire visible spectrum [40,58,84]. Halide mixing can help stabilize the cubic phase at working temperatures, while the increased bandgap that is achievable with these mixtures facilitates their applications as top cells in tandem solar cells [94].

In many aspects, the physical properties of inorganic halide perovskites are quite similar to the organic–inorganic hybrid counterparts. Using density functional theory (DFT)-based calculations, Berdiyorov *et al.* reported that the optoelectronic properties of hybrid perovskites do not change much when the organic cation is replaced by inorganic Cs^+ [86]. As shown in Fig. 1(b), the real part of the dielectric function, absorption coefficient, and reflectivity demonstrate the similar tendency between $MAPbI_3$ and $CsPbI_3$. Nicholas *et al.* reported, for the first time, the fundamental properties of all-inorganic perovskites, such as its exciton binding energy, reduced mass, dielectric screening, and the phase transition through low-temperature magneto transmission spectroscopy [87]. The variation of bandgap in all-inorganic perovskite under different temperatures is illustrated in Fig. 1(c). They observed the red shift of bandgap energy with more Br^- replaced by I^-, corresponding to the experimental observation of the reduced bandgap with a heavier halide substitution.

The optical transitions and charge transfer in perovskite materials are also greatly hinged on their electronic properties. In typical 3D inorganic perovskites, the valence bands are contributed by the Pb 6s orbital and the p orbitals of the halide ions, while the halide p orbitals play the dominant role. On the other hand, the conduction band is determined by the antibonding mixing of the dominant Pb 6p orbital and the halide p orbitals [88,95]. The calculated electronic structures of inorganic perovskites are depicted in Figs. 1(d) and 1(e). The electronic states are only slightly affected by the Cs^+ cations in inorganic perovskites, thus making no essential impact on the bandgaps. In addition, all-inorganic perovskites exhibit direct bandgaps, indicating their promising light-response behavior [40]. However, the Rashba effect can lead to an indirect nature of bandgaps in perovskites. Marrionnier *et al.* found that similar to hybrid perovskites, inorganic perovskite $CsPbI_3$ displays an indirect bandgap under the influence of the Rashba effect [96,97]. The Cs^+ cation has a negligible direct influence on the electronic structure near the band edge, but it produces an indirect effect through the tilting of PbX_6 octahedra, affecting the excitation and recombination of electrons and holes. Moreover, the identical effective mass of electrons and holes, as indicated in Fig. 1(d), contributes to high carrier mobilities in the material. As the halide composition moves from iodide to chloride, the energy levels of the halide p orbitals lower, triggering the shift of the valence band toward more positive potentials. The valence band positions of $CsPbBr_{1.5}I_{1.5}$, $CsPbBr_3$, and $CsPbBr_{1.5}Cl_{1.5}$ are calculated to be 6.1, 6.5, and 6.5 eV, while the conduction bands are 4.3, 4.15, and 3.8 eV, respectively [98]. The bandgap variations among different halide compositions can be regarded as an important factor contributing to the halide segregation phenomena. This will be discussed in the mechanism section.

The calculation for effective mass and exciton binding energies was reported by analyzing the magnetic field dependence of hydrogenic and free carrier transitions [87]. The exciton binding energy of $CsPbBr_xI_{3-x}$ increases with the Br content. Compared to the exciton energy of $MAPbI_3$ (16 ± 2 meV), $CsPbI_3$ shares a similar value of 15 ± 1 meV, while it increases to 22 ± 3 meV for $CsPbI_2Br$ and 33 meV for $CsPbBr_3$. Figure 1(f) illustrates the values of exciton binding energy, effective mass, and effective dielectric constant for Cs-based inorganic perovskites with different bandgaps (halide compositions). In general, the carrier effective mass increases with the bandgap, indicating the significant influence of the halide anions on the electronic properties of perovskites.

For mixed-halide perovskite NCs, when the size of perovskite crystals is smaller than the Bohr radius, the quantum confinement effect takes place [99]. Compared to bulk films or single crystals, perovskite NCs present improved optical and electronic properties due to their low trap densities, high surface-volume ratio, and versatile functionalization. The versatile tunability of

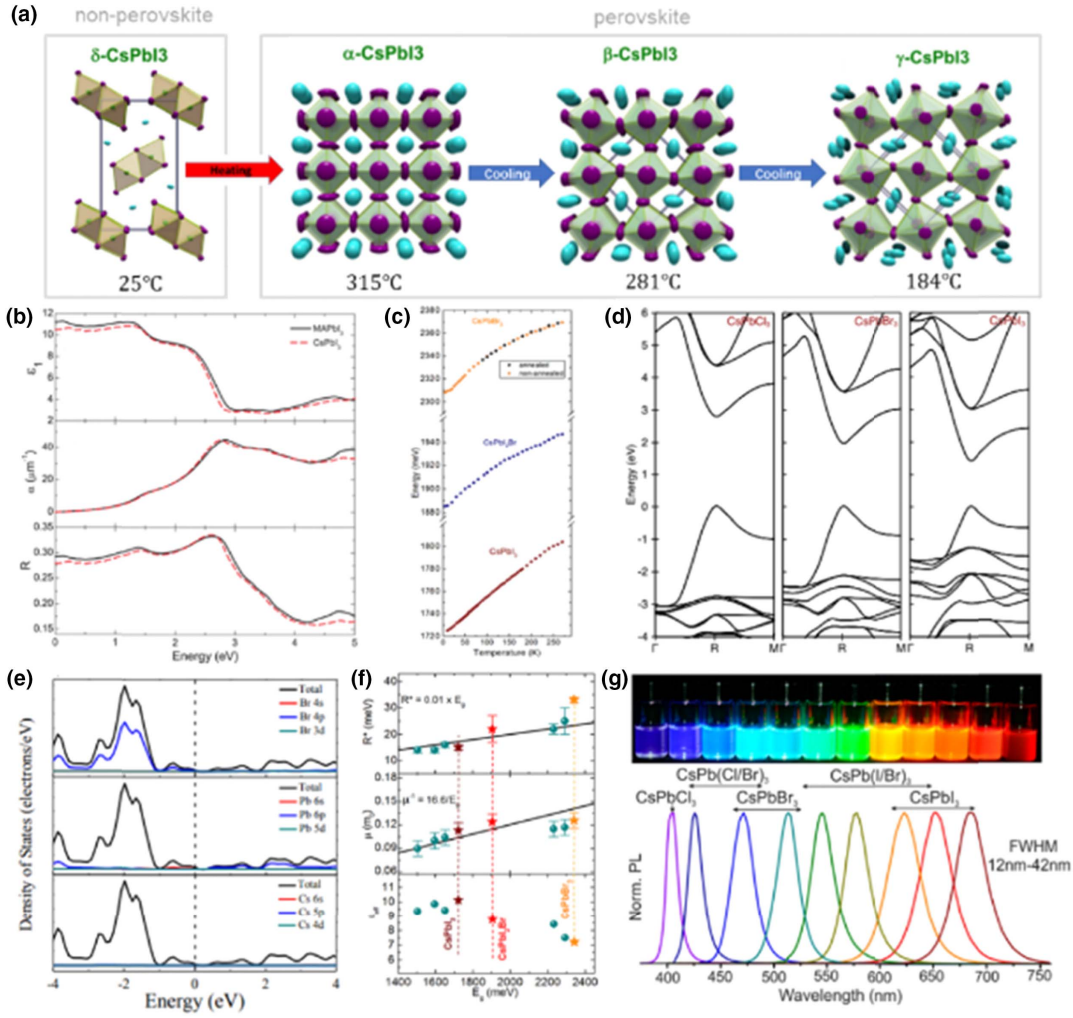

Fig. 1. (a) Structural transition of the $CsPbI_3$ material at different temperatures. Reproduced with permission [45], Copyright 2018, American Chemical Society. (b) Real part of dielectric function (ε_1), absorption coefficient (α), and reflectivity (R) of $MAPbI_3$ and $CsPbI_3$ perovskites. Reproduced with permission [86], Copyright 2016, American Chemical Society. (c) Energy of the 1s transition (reflecting the evolution of the band gap) as a function of temperature for $CsPbI_3$, $CsPbI_2Br$, and $CsPbBr_3$ perovskites. Reproduced with permission [87], Copyright 2017, American Chemical Society. (d) The calculated electronic band structures for the $CsPbCl_3$, $CsPbBr_3$, and $CsPbI_3$ (cubic phase), including relativistic corrections, from density functional theory. Reproduced with permission [40], Copyright 2015, American Chemical Society. (e) Density of states of the cubic $CsPbBr_3$ with corresponding contributions of elements to energy band. Reproduced with permission [88], Copyright 2016, Wiley-VCH. (f) Binding energy (R^*), effective mass (μ), and dielectric constant (ε_{eff}) as a function of the band gap. Reproduced with permission [87], Copyright 2017, American Chemical Society. (g) Images and PL spectra of the perovskite colloidal solutions in toluene with different halide compositions. Reproduced with permission [40], Copyright 2015, American Chemical Society.

emission and absorption is retained in perovskite NCs via halide engineering from $CsPbCl_3$, $CsPbBr_3$ to $CsPbI_3$. Figure 1(g) illustrates the tunable light emission and the PL spectra in different NC solutions [40].

3. PHASE SEGREGATION IN ALL-INORGANIC PEROVSKITES

A. Phenomena of Phase Segregation

The phase-segregation phenomenon was first discovered in 2015 by Hoke *et al.* in $MAPb(Br_xI_{1-x})_3$ with x ranging from 0.2 to 1 [48]. They observed alternation of the PL spectra and the X-ray diffraction (XRD) pattern of the perovskite film after being exposed to light illumination. Figure 2(a) illustrates the observed red shift of the PL spectra of the $MAPb(Br_{0.4}I_{0.6})_3$ film with an illumination duration of 45 s [48]. Interestingly, the XRD patterns, PL, and absorption spectra can be reversed to their preliminary states after leaving the material in dark conditions for a few minutes, signifying that the phase segregation in hybrid perovskites is fully reversible.

Following the first observation, several experiments focusing on the phase segregation of all-inorganic perovskites and the comparison of them with the organic–inorganic hybrid perovskite have been reported. Up to now, almost all of the optical investigation on the phase segregation in all-inorganic perovskite is based on the analyses of PL spectra.

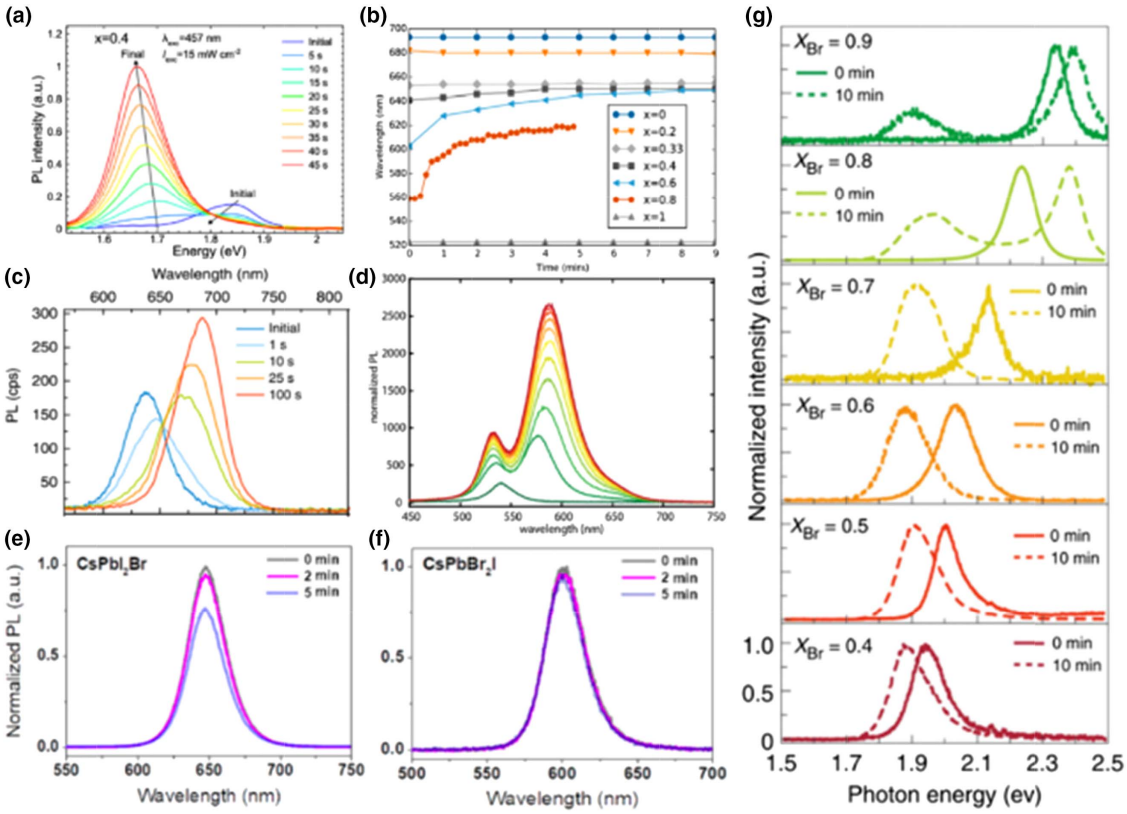

Fig. 2. (a) PL spectra of the $MAPb(Br_{0.4}I_{0.6})_3$ thin film over 45 s in 5 s increments. Reproduced with permission [48], Copyright 2015, RSC Publishing. (b) Time-dependent PL peak position in $CsPb(Br_xI_{1-x})_3$ of different halide compositions. Reproduced with permission [100], Copyright 2016, American Chemical Society. (c) PL spectra of $CsPb(Br_{0.5}I_{0.5})_3$ film with the illumination duration of 100 s. Reproduced with permission [52], Copyright 2017, Nature Publishing Group. (d) PL spectra of $CsPb(Br_{0.1}I_{0.9})_3$ with the illumination duration of 10 min. Reproduced with permission [50], Copyright 2017, American Chemical Society. PL spectra with the illumination of 5 min of the (e) $CsPbI_2Br$ and (f) $CsPbBr_2I$ films. Reproduced with permission [65], Copyright 2017, American Chemical Society. (g) PL spectra of the $CsPb(Br_xI_{1-x})_3$ with x ranging from 0.4 to 0.9. The solid lines were the spectra taken from freshly made samples, and the dashed lines were measured after 10 min illumination. Reproduced with permission [61], Copyright 2019, Nature Publishing Group.

Rachel *et al.* conducted the first PL experiment investigating the illumination stability of spin-coated mixed-halide perovskites $CsPb(Br_xI_{1-x})_3$ with a series of halide compositions [100]. They reported stabilized PL spectra in films with $0 \le x \le 0.33$ and red shift of the spectra in films with $0.33 < x < 1$ during the whole course of illumination (100 mW/cm^2 intensity), as shown in Fig. 2(b), indicating a wider range of stable perovskite compositions against phase segregation in all-inorganic perovskites. Although, other reports indicate a stabilized PL in the $0.2 < x < 0.4$ region [100].

Hoke *et al.* showed that for a mixed-halide perovskite, $x = 0.6$, that had undergone phase segregation, the resulting absorption peak after light soaking resembled that of the same material if 1% of it had turned into perovskite with $x = 0.2$. XRD measurements were performed before and after light soaking to analyze the presence of minority domains in the film and revealed that the emissive minority phase, with improved iodide content of 0.2, makes up approximately 23% of the material [48]. These results helped reveal that minority domains suffer from more anisotropic strain and that various stoichiometries often result in an emission that resembles an $x = 0.2$ perovskite after illumination [100].

Draguta *et al.* also discovered a red-shifted PL signal from 637 nm to 687 nm in spin-coated $CsPb(Br_{0.5}I_{0.5})_3$ film after 100 s with the excitation fluence of 60 mW/cm^2 [Fig. 2(c)] [52]. A similar PL red shift was also observed by Bischak *et al.* from ~545 nm to ~600 nm in $CsPb(Br_{0.1}I_{0.9})_3$ after being illuminated by one sun for 10 min, as illustrated in Fig. 2(d) [50]. The film was also prepared via the spin-coating method. However, the author did not explain the abnormal PL peak position since the inorganic perovskite film with such a high iodine concentration should possess an initial PL peak at around 690 nm [100]. Moreover, the I-rich peak after phase segregation located at 600 nm did not correspond to any I-rich inorganic perovskite compositions but seems to be contributed by $CsPb(Br_{0.6}I_{0.4})_3$.

Interestingly, by the direct comparison of the light response behavior between hybrid and all-inorganic perovskites, Zhou *et al.* observed no change on the PL peak position for $CsPbI_2Br$ and $CsPbIBr_2$ thin films after being exposed to light illumination with the intensity of 10^4 mW/cm^2 [Figs. 2(e) and 2(f)], while the hybrid $MAPb(I_{0.5}Br_{0.5})_3$ film exhibits a red shift of the PL spectra in 6 s [65]. Although the films are prepared by using a similar spin-coating method, Zhou *et al.*

used a sapphire substrate and DMF solvent instead of glass and DMSO. The weaker polarity of DMF and different electronegativity of the sapphire surface compared to glass may result in different film quality. For example, more electronegative substrates prefer to form covalent bonds with the applied film, which yields films with higher ion mobilities [101]. Similarly, the polarity of the solution can favor the complexation of one halide species leading to a halide imbalance, both of which promote phase segregation [73].

A similar controversial observation is also discovered in the case of vacuum deposited all-inorganic perovskite films. Gao *et al.* observed that the iodine-rich peaks located at around 1.87 eV appeared after 10 min illumination once the x values of $CsPb(Br_xI_{1-x})_3$ films are larger than 0.4, as illustrated in Fig. 2(g) [61]. This result of the PL peak position is consistent with the experimental data from Rachel's group [100]. However, Ma *et al.* reported the deposition of $CsPbIBr_2$ thin film using dual-source thermal evaporation, and the stabilized PL characterization explained the absence of halide phase segregation [78]. The different observations also stem from the substrate materials in these two reports. Gao *et al.* used conventional glass as the substrate while Ma *et al.* utilized a TiO_2-coated glass substrate to prepare the perovskite films. Because phase segregation is strongly related to photoexcited electrons [50,52], the use of a TiO_2 transport layer could suppress phase segregation via the dissipation of the photogenerated carriers, something we will further discuss in the mechanism section. The grain boundaries within the perovskite thin film are believed to play a vital role in phase segregation. Direct visualization of perovskite films via cathodoluminescence mapping revealed that phase segregation mainly happened at the grain boundaries, as illustrated in Fig. 3 [50,58]. Even for single crystal platelets, the phase segregation has more chance to take place at the edge of the platelet rather than at the center [102]. Chen *et al.* also visualized the ionic transport in $CsPbBrI_2$ thin films via fluorescence lifetime imaging and observed that bromide vacancies diffuse toward the dark area, resulting in the emergence of the I-phase PL in the remote dark region [103].

Besides thin films, phase segregation is also observed in all-inorganic perovskite NCs. Zhang *et al.* investigated phase segregation in $CsPb(I_{0.6}Br_{0.4})_3$ high-density NC ensemble films and isolated perovskite NCs. As illustrated in Fig. 4(a), a blue peak shift was observed in PL spectra from 635 nm to 618 nm for the $CsPbI_{1.8}Br_{1.2}$ NC ensemble film after 10 min illumination, and that was reversible in the dark. A similar blue shift is also discovered from 615 nm to 515 nm after 50 min illumination in isolated perovskite NCs, but it is not reversible in dark conditions [Fig. 4(b)] [62]. In another controversial case, Draguta *et al.* discovered stabilized PL spectra for the $CsPb(I_{0.5}Br_{0.5})_3$ NC film when it was illuminated with 60 mW/cm^2 blue light for 120 s [Fig. 4(c)] [52]. As shown in Fig. 4(d), Mora-Sero *et al.* also observed that the PL peak wavelength remains constant in $CsPb(I_xBr_{1-x})_3$ NC films after being illuminated with the intensity of 10 mW/cm^2. The only blue shift case discovered by Zhang *et al.* can be ascribed to the extremely intense excitation light intensity of 30 W/cm^2 and even 15 kW/cm^2. Such high-intensity several orders of magnitude higher than one sun illumination can cause the

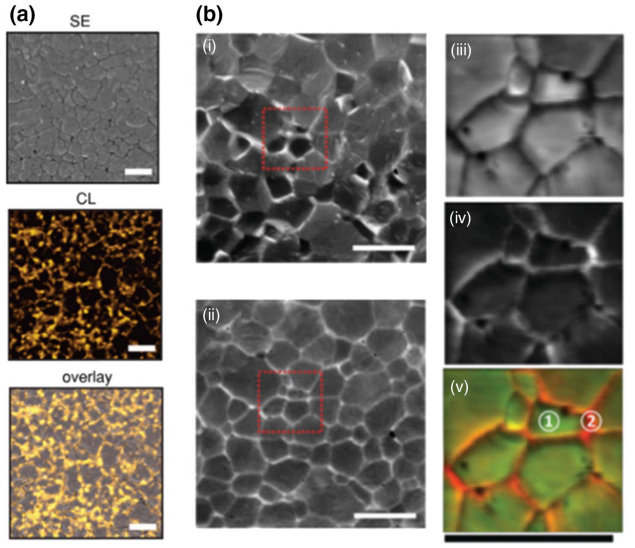

Fig. 3. (a) Secondary electron (SE), cathodoluminescence (CL), and SE/CL overlay of the $MAPb(I_{0.1}Br_{0.9})_3$ film. The scale bar is 2 μm. Yellow-colored spots represent the signal from the I-rich clusters. Reproduced with permission [50], Copyright 2017, American Chemical Society. (b) Imaging the phase segregation in the $CsPbIBr_2$ film: (i) secondary electron SEM image; (ii) CL mapping; (iii) and (iv) are the enlarged image of the highlighted area in (i) and (ii), respectively; (v) color-coded emission mapping of the film, where the orange regions have longer wavelength emission than the green region, indicating the accumulated iodine ions in the orange area. Reproduced with permission [58], Copyright 2017, Wiley-VCH.

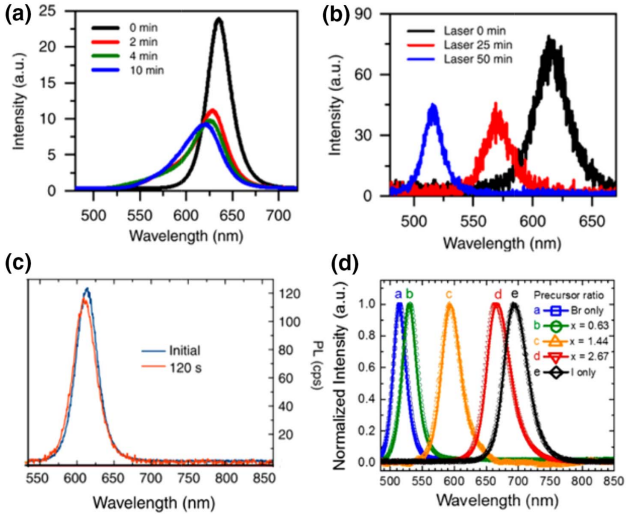

Fig. 4. (a) PL spectra measured at 0, 2, 4, and 10 min for one position of the $CsPbBr_{1.2}I_{1.8}$ ensemble film excited at a laser power density of 30 W/cm^2 [62]. (b) PL spectra measured up to 50 min for one position of the single $CsPbBr_{1.2}I_{1.8}$ NC excited at a laser power density of 6 W/cm^2. Reproduced with permission [62], Copyright 2019, Nature Publishing Group. (c) PL spectra of $CsPb(Br_{0.5}I_{0.5})_3$ NCs film with the illumination duration of 120 s. Reproduced with permission [52], Copyright 2017, Nature Publishing Group. (d) Normalized PL spectra of the $CsPb(Br_xI_{1-x})_3$ NCs for 10 min. The dots represent the initial spectra while the lines represent the spectra after 10 min. Reproduced with permission [63], Copyright 2019, American Chemical Society.

sublimation of iodine ions, which will trigger irreversible material degradation into Br-rich compositions, leading to the blue shift of PL peaks [62].

B. Impacts of Phase Segregation on the Performance of Optoelectronic Devices

From a practical point of view, phase segregation has a significant influence on the performance of mixed-halide optoelectronic devices. To date, although most research investigating the effect of phase segregation on perovskite optoelectronic device performances is based on hybrid perovskites, they can also help scientists understand the influence in all-inorganic perovskite devices since the segregation mechanisms are not directly linked to the A cations. Generally, phase segregation has a negative influence on the solar cell performance parameters. Braly *et al.* observed the reduction of V_{OC} as a consequence of phase segregation [56]. They claimed that the impact comes from three aspects. First, the red shift of the band edge causes increased thermalization losses in the perovskite active layer, such as the potential energy loss of carriers when they move from large-bandgap domains to small-bandgap domains. Second, the segregated clusters will suppress the charge carrier collection due to the carrier recombination at small-bandgap I-rich domains. Third, the transient band edge caused by phase segregation will affect the effective absorption matching in two-terminal tandem solar cells since the altered transmissivity of the perovskite top cell will cause the absorption variation in the bottom cell. Duong and coworkers also observed the reduction of V_{OC} and fill factor (FF) along with an increase of hysteresis within the mixed-halide perovskite solar cells after solar illumination for 12 h [104]. Meanwhile, a slight increase in J_{SC} was observed since the absorption band edge was extended as a result of the red-shifted bandgap. Similar hysteresis behavior was also observed by Li *et al.* in $CsPbIBr_2$-based solar cells while absent in the phase-segregation-free composition of $CsPb_{0.75}Sn_{0.25}IBr_2$ [105]. Kamat *et al.* observed simultaneously dropped V_{OC} and J_{SC} upon phase segregation, which is attributed to the enhanced hole accumulation and charge recombination in the I-rich region [67].

Phase segregation can also affect the interfacial condition between perovskite and charge transport layers in solar cells. Li *et al.* and Hu *et al.* suggested that the phase segregation enhanced ion movement arouses the accumulation of anions at perovskite/charge extraction layer interfaces, creating barriers against the collection of photogenerated charge carriers [58,68]. This accumulation process will also screen the built-in electric field inside the perovskite layer and cause significant J–V hysteresis of the solar cells.

Phase segregation is also an essential issue to consider in the case of LEDs. Braly *et al.* and Duong *et al.* reported the current-induced phase segregation in hybrid perovskites under a dark condition [56,104]. The altered emission spectra caused by phase segregation will significantly limit the performance of LED devices and the potential color design. As aforementioned, all-inorganic perovskite NCs are promising candidates for light-emitting devices. Research on bias-induced phase segregation in all-inorganic perovskite NCs has been conducted by Zhang *et al.* [62]. The PL peak was found to blue shift from 631 nm to 607 nm in $CsPbBr_{1.2}I_{1.8}$ NCs under a bias of 10 V for 4 min, which can be reversed by dark treatment and opposite electrical bias. These observations demonstrate that fabricating mixed-halide perovskite LED devices without suppressing the phase segregation can cause devastating uncertainty of emission color.

C. Plausible Mechanisms of Phase Segregation

Up to now, several models have been proposed to explain the driving forces of phase segregation. The theoretical descriptions can be categorized into three categories. The first one is the analysis of thermodynamic phase diagrams to illustrate the preferred phase segregated state under illumination [59,61]. The second mechanism is based on the electron–phonon-coupling-induced lattice strain, which triggers the formation and enlargement of halide clusters. These two mechanisms have been cited in studies involving both all-inorganic perovskites and hybrid perovskites [50,61,106]. The third mechanism is based on defects and charge traps interacting with photogenerated charge carriers, and the associated local electric field is often considered as an important factor [107,108]. Although the third mechanism was proposed to explain the observation of phase segregation in hybrid perovskites, it provides insights on the similar phenomena in inorganic perovskites since charge traps are ubiquitous.

Brivio and coworkers carried out a thermodynamic analysis to shed light on phase segregation in mixed-halide perovskites [59]. They proposed that the light illumination tends to alter the free energies, leading to destabilization of the uniformly distributed halide states. Figure 5(a) illustrates the miscibility gap of $MAPb(Br_xI_{1-x})_3$ for $0.3 < x < 0.6$ at 300 K, where the material is unstable. The authors claimed that annealing above room temperature and less than 373 K could generate uniform halide states of perovskite films, but the light illumination can act as an additional energy source to assist overcoming the halide segregation kinetic barrier. However, this model does not explicitly consider the effect of light illumination on the phase diagram; thus, it cannot explain the reversibility of phase segregation in the dark. Furthermore, the halide composition dependence of the formation energy of $CsPb(Br_xI_{1-x})_3$ was later investigated through first-principles calculations [109], suggesting that the stable configurations can be obtained across the whole range of halide mixing, but the effect of light illumination remains elusive [Fig. 5(b)].

In the work by Draguta *et al.*, the effect of light illumination was taken into consideration as an additional energy term that modifies the curve of the formation energy. They reported that the driving force of phase segregation is greatly related to the bandgap discrepancies between the uniform state, the Br-rich domains, and the I-rich domains [52]. They calculated the formation energy of the mixed state of $MAPb(I_{1-x}Br_x)_3$, as shown in Fig. 5(c). The formation energy ΔE_{GS} was shifted from zero to a negative level after introducing the temperature term $T\Delta S$ at 300 K and further became positive after single-photon absorption ΔE_g is introduced. The formation energy calculation was extended to all-inorganic perovskites by Wang *et al.* [61]. Figure 5(d) illustrates the alternation of the Gibbs free energy in darkness (blue line) and under illumination (orange line), showing partially positive free energy after the film is illuminated. In general, the analysis of the thermodynamic driving

force explains well the dependence of reversible phase segregation on the halide content and is consistent with the experimental results.

In the second category of the mechanism, polaron-induced lattice deformation is cited as the driving force of phase segregation. Bischak *et al.* proposed the formation of polaron in the framework of the electron–phonon coupling as a result of the hole localization in the randomly formed I-rich domains [50]. The formation of polaron would cause lattice strain and trigger the migration of iodine ions toward segregated clusters, as is illustrated in Fig. 5(e). In order to release the lattice strain, the I-rich domains will migrate to the grain boundaries, explaining the observation of long-wavelength emission at the grain boundaries. Interestingly, they observed that replacing MA^+ cation with Cs^+ can increase the lattice stability and suppress the polaron-induced lattice deformation [106]. Figure 5(f) illustrates the evolution of phase composition over time with the presence of polaron in hybrid and inorganic perovskite films, indicating the better stability against phase segregation of the Cs^+-based perovskites. The authors proposed that this phenomenon stems from the weakly bounded polaron in inorganic perovskites, resulting in a smaller strain field and weakening the driving force of phase segregation. This conclusion resonates with the previous phenomenological theory that the suppressed electron–phonon coupling contributes to the weak polarizability of the inorganic perovskite lattice [110].

In a recent work, Wang *et al.* combined thermodynamic and lattice deformation models, claiming that polaron-induced lattice strain is the origin of phase segregation [61]. Specifically, polarons can introduce excessive strain energy due to the locally distorted lead-halogen bonds, leading to the positive formation energy shown in Fig. 5(d). To sum up, phase segregation is a process releasing the strain energy through the formation of I-rich and Br-rich clusters.

The last model is based on electronic traps and the associated electric field in the perovskite films. Knight *et al.* pointed out the key role of a localized electric field generated from electrons and holes in the trap states that tends to interact with charges defects and cause the migration of anion vacancies to the trapped electrons [107]. The illustration of the band diagram is presented in Fig. 5(g). The authors proposed two other species of defects: one has an intrinsically neutral charge that is a result of lattice distortions near grain boundaries, and the other arises due to interstitial halide ions or halide ion vacancies with low mobility. The latter species has been proposed by numerous studies to be responsible for J–V hysteresis in mixed-halide perovskite photovoltaic devices. They found that by varying the intensity of light illuminating the mixed-halide perovskite film and controlling the total number of incident photons, the fraction of charge carriers that recombined through trap states was directly related to the severity of the halide segregation observed. A variation in PL was observed when the bias

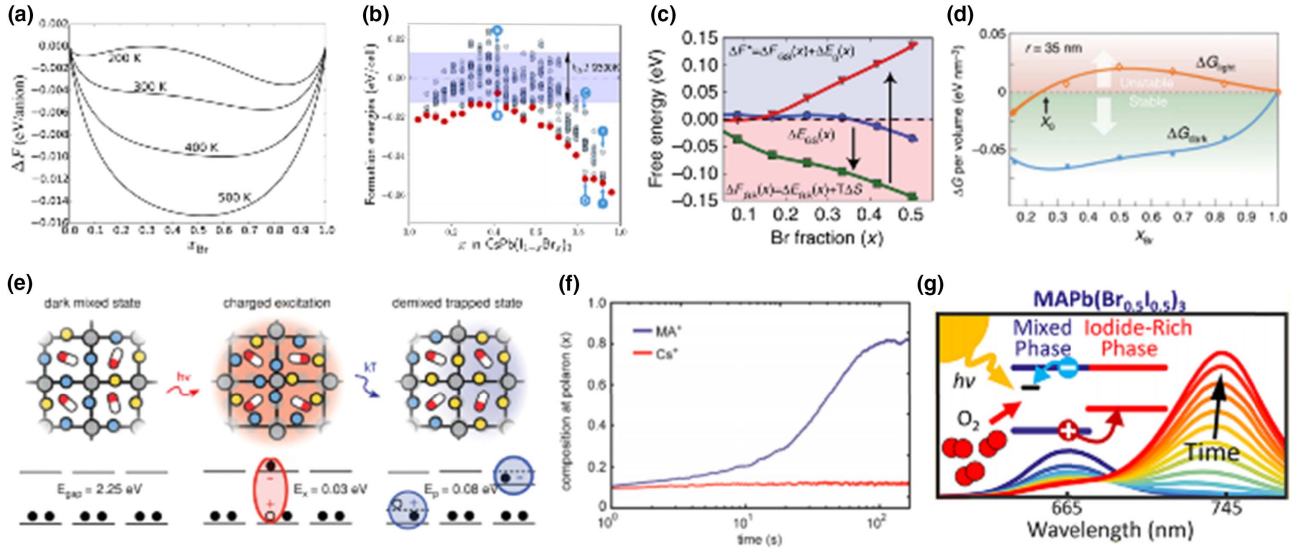

Fig. 5. (a) Helmholtz free energy of the $MAPb(Br_xI_{1-x})_3$ perovskite as a function of the bromide concentration and temperature. Reproduced with permission [59], Copyright 2016, American Chemical Society. (b) Formation energy landscape of the $CsPb(Br_xI_{1-x})_3$ as a function of the bromide concentration. The configuration with a given x is illustrated by the grey dots and the lowest energy configuration is highlighted in red. Reproduced with permission [109], Copyright 2020, American Chemical Society. (c) Free energy of formation as a function of x in the $MAPb(Br_xI_{1-x})_3$ material. The blue lines represent the 0 K ground state formation energies. The green line is the free energies at 300 K. The red line represents the free energy after single photon absorption. Reproduced with permission [52], Copyright 2017, Nature Publishing Group. (d) Calculated Gibbs free energy of the $CsPb(Br_xI_{1-x})_3$ perovskite with (orange line) and without illumination (blue line). Reproduced with permission [61], Copyright 2017, Nature Publishing Group. (e) Photo-induced polaron trapping and associated energy scales related with light-induced phase segregation. Yellow spheres represent I ions, blue spheres represent Br ions, and pill shapes represent the MA cation. Reproduced with permission [50]. Copyright 2017, American Chemical Society. (f) Simulated time trace of the composition at the polaron for $MAPb(I_{0.15}Br_{0.85})_3$ and $CsPb(I_{0.15}Br_{0.85})_3$. Reproduced with permission [106], Copyright 2018, American Chemical Society. (g) Schematic illustration of the band diagram and carrier migration due to trap states in perovskite thin films. Evolution of the perovskite PL spectra upon illustration. Reproduced with permission [107], Copyright 2018, American Chemical Society.

was varied on the device, indicating the movement of charged trap states and, to a lesser extent, the variation in current in the device [107].

Belisle *et al.* also discovered a similar process happening at the perovskite surface, which leads to phase segregation [108]. Although this model is empirically based on hybrid perovskites, they observed that phase segregation could be strongly affected by the perovskite surface passivation. The phase segregation in inorganic perovskites may also stem from the interaction of defects and generated local electric fields since there are plenty of trap states in both films and NC surfaces if no passivation process is introduced.

The role of shallow defect states must be explored to fully understand the role of trap states in phase segregation. Guo *et al.* found that for films of (FA,MA,Cs) $Pb(I_{1-x}Br_x)_3$, iodide ions accumulate near positive charges at the intermixed shallow states. Their results imply that shallow states of intermixed halides form iodide-rich, low bandgap domains. This means that the mechanism for the formation of iodide-rich domains is different for mixed-cation mixed-halide perovskites from single-cation perovskites. Iodide-rich domains typically form at the grain boundaries of illuminated sites [54,111]. They also investigated the thermal dependence of the occupancy of shallow states and proposed that lowering the temperature results in more charge carriers occupying these shallow states, resulting in a longer carrier lifetime due to hindered recombination [112]. Sarritzu *et al.* confirmed this correlation by reporting an increase in the radiative recombination rate with decreasing temperature [97].

D. Mitigation Methods

Halide segregation in mixed-halide perovskites may deteriorate the performance of optoelectronic devices. Here, we summarize the proposed strategies to mitigate the light-induced phase segregation in all-inorganic perovskites. In general, there are three approaches toward suppressing phase segregation in mixed-halide perovskites. Compositional tuning has been demonstrated to stabilize the perovskite lattice [16,104,106]. Second, morphological engineering via crystallinity enhancement has shown more promising results through the suppression of grain boundaries [57,58,113]. Lastly, passivation of trap states can significantly suppress phase segregation by eliminating ion vacancies [108,114–116]. Some mitigation strategies were reported based on hybrid perovskites but might be also suitable in the case of inorganic perovskites. Additionally, it is worth noting that choosing the inorganic perovskite itself has been regarded as one strategy suppressing the phase segregation. Mitigation methods should aim to increase the energy barrier for halide migration, limiting lattice strain and electron–phonon coupling and reducing the trap states.

Since the phase segregation is considered a thermodynamic process in mixed-halide perovskite, temperature control should be an effective approach in adjusting the rate of phase segregation. Theoretical calculations suggest that the affinity of mixed-halide ions increases with rising temperature, resulting in superior photostability at a higher temperature [50,59]. Wang *et al.* investigated the light response behavior of $CsPb(Br_xI_{1-x})_3$ NCs embedded in a $Cs_4Pb(Br_xI_{1-x})_6$ matrix under an extremely intense illumination of 4400 sun at different temperatures [61]. At low temperatures, an additional peak located at smaller energy appears after several hours of illumination, while the PL spectrum remains stable at elevated temperatures, demonstrating strong temperature dependence of photostability in the perovskite. However, high temperatures may trigger a fast halide segregation process, which was corroborated by the experiment by Barker *et al.* and some other groups [48,54]. Clearly, the debate on temperature-dependent entropy mixing and ionic transport remains unsolved and requires further research.

Triple and quadruple cation perovskite compositions with additional FA^+ and Rb^+ are reported to be the most stable against phase segregation [104,117]. Bi *et al.* reported a hybrid mixed-cation perovskite (MA/FA) device that exhibited a PCE of 20.8% along with an external quantum efficiency of 0.5%, a record for perovskite photovoltaics at the time [118]. The incorporation of inorganic cations such as Cs^+ and Rb^+ into the A site has shown to improve solar cell performance, increase charge carrier mobility, and passivate trap states. Hu *et al.* reported that a quadruple-cation perovskite exhibited the best PCE over 5 min under constant illumination when compared to the organic cations or solely Cs^+. They showed that the quadruple-cation perovskite exhibited superior charge transport, and the inorganic cations dramatically reduce trap state density [119].

Besides the engineering of an A-site cation, mixing the B-site Pb^{2+} ions with Sn^{2+} has also been proposed as an efficient strategy against phase segregation [53,105]. In the case of all-inorganic perovskites, Li *et al.* discovered that the PL peak position remains stable for $CsPb_{0.75}Sn_{0.25}IBr_2$ after 15 min illumination while the red-shifted PL is discovered for $CsPbIBr_2$ films under the same circumstances [Fig. 6(a)] [120], indicating the replacing of 25% Pb^{2+} ions by Sn^{2+} can improve the stability of mixed-halide perovskite against phase segregation. This observation is similar to the result that Yang *et al.* obtained in hybrid perovskite [53]. The superior stability of the lead–tin mixed perovskites can be attributed to the different properties of the Sn-halide bond compared to the Pb-halide bond, leading to the suppressed extent of halide segregation.

Ginsberg and coworkers reported limited electron–phonon coupling when the MA^+ is replaced by Cs^+ because of the more solid lattice structure in inorganic perovskites that suppresses the lattice distortion [106]. Some other groups also reported the narrowing of an unstable phase segregation range of bromide concentration when MA^+ is partially substituted by Cs^+ [16,56].

Crystallinity enhancement is regarded as another approach toward suppressing the phase segregation in mixed-halide perovskites. It was reported by several groups that larger grain size in perovskite films results in better stability against phase segregation [56,57,113,121]. The origin of this stability enhancement is the reduced density of grain boundaries, where halide ions are reported to accumulate [50,58]. The ionic mobility of halide perovskite is relatively higher along the grain boundaries than inside the bulk crystal [122,123]. As mentioned in the mechanism section, grain boundaries are filled with trap states facilitating the segregation of halide

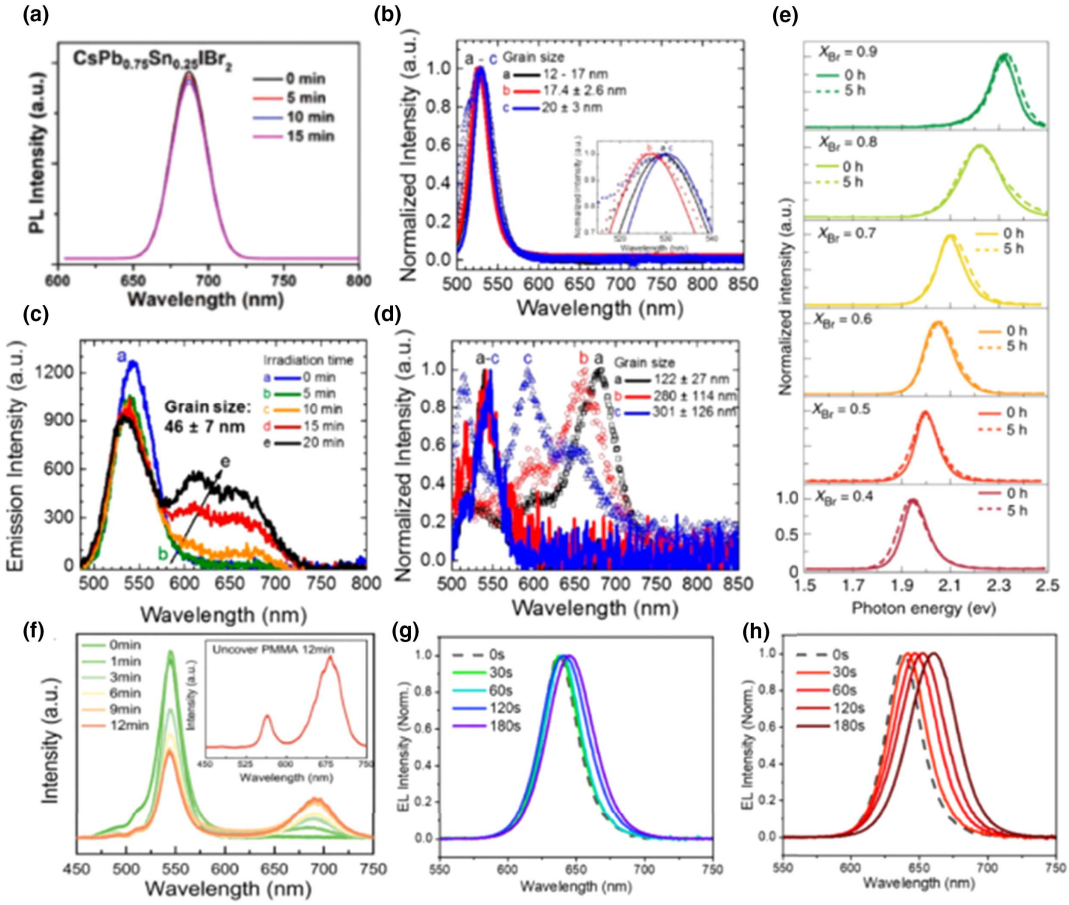

Fig. 6. (a) Steady-state PL spectra of the $CsPb_{0.75}Sn_{0.25}IBr_2$ perovskite with different illumination time. Reproduced with permission [105], Copyright 2018, Wiley-VCH. Normalized PL spectra of the $CsPbBr_{0.37}I_{0.63}$ bulk films with grain size of (b) up to 19.5 nm, (c) 46 ± 7 nm, and (d) greater than 100 nm. Reproduced with permission [63], Copyright 2019, American Chemical Society. (e) The PL spectra of the $CsPb(Br_xI_{1-x})_3$ material embedded in the $Cs_4Pb(Br_xI_{1-x})_6$ matrix with the illumination duration of 5 h. Reproduced with permission [61], Copyright 2019, Nature Publishing Group. (f) The PL spectra of the $CsPb(Br_xI_{1-x})_3$ microplatelet covered with PMMA layer with the continuous illumination for 12 min. Inset shows the spectra of the platelet without PMMA encapsulation after illuminated for 12 min. Reproduced with permission [120], Copyright 2019, RSC Publishing. (g) Normalized electroluminescence spectra of the red LED based on $CsPb(Br_xI_{1-x})_3$ NCs at a driving voltage of 5 V (g) with and (h) without KBr passivation. Reproduced with permission [115], Copyright 2020, American Chemical Society.

ions. Hence, the reduction of grain boundary density can effectively reduce the amounts of the strain centers for halide segregation.

The suppression of photo-induced phase segregation within all-inorganic perovskite is also possible through shrinking of the perovskite crystals to NCs. According to Andrés *et al.*'s report, the threshold grain size of phase separation is 46 ± 7 nm, corresponding to the diffusion length of perovskite [63]. When the perovskite grain size is larger than the threshold, the electron/hole mobility would not be confined in the grain, and the charge would diffuse with its own diffusion length. This study provides the transition of phase segregation from NC to bulk, as no phase separation was observed for the NC film with various grain sizes up to 19.5 nm [Fig. 6(b)], but it appeared in bulk films with grain sizes of 46 ± 7 nm or greater after 20 min of irradiation [Fig. 6(c)]. In comparison, films with larger grain sizes (from 122 ± 27 to 301 ± 126 nm) show severe phase segregation under irradiation [Fig. 6(d)]. The effect of crystal size was also investigated by Wang *et al.*, who reported that for $CsPb(Br_xI_{1-x})_3$ NCs, the photo-induced phase separation was largely suppressed when embedded in nonperovskite $Cs_4Pb(Br_xI_{1-x})_6$ endotaxial matrices [61]. Figure 6(e) illustrates the stabilized PL spectra of the embedded perovskite NCs. They also claimed that the sizes of NCs and host–guest interfaces are critical for the photostability of perovskites. NCs with the crystal diameter of 7.5 nm showed superior photostability compared to the 35 nm crystals, possibly attributed to Gibbs free energy equation that the NCs size has to reach a critical value for the volume proportional term to dominate and phase segregation to prevail. This result is consistent with the size magnitude reported by Andrés *et al.* [63].

The charge traps in perovskite material are also related to phase segregation, resulting in an effective strategy of trap state passivation to increase the photostability of perovskites. According to Abdi-Jalebi *et al.*'s report, after introducing potassium iodine into the precursor solution as the passivation agent for perovskite synthesis, the PL peak shift in $(Cs_{0.06}MA_{0.15}FA_{0.79})Pb(Br_xI_{1-x})_3$ material is eliminated with

the illumination duration of 30 min [114]. They claimed that the excessive iodine ions provided by the potassium iodine can reduce the number of iodine vacancies and suppress the halide ion mobility. Moreover, the potassium ions were observed to accumulate near the grain boundaries and passivate the trap states, leading to the repression of phase segregation. Zheng *et al.* even reported that the potassium triggered passivation effect can also be induced by the light illumination [124]. Furthermore, Yuan *et al.* conducted experiments to passivate deep trap states by adding a $Pb(NO_3)_2$ methyl acetate solution to a $CsPbI_2Br$ perovskite film. They observed that the trap state density of the perovskite decreased from 8×10^{16} to 6.64×10^{16} cm^{-3} after the passivating agent was added [125]. A bunch of passivation agents were also introduced by other groups such as potassium bromide, polymethyl methacrylate (PMMA), tri-iodine molecules, and trioctylphosphine oxide [108,115,116,120]. Wang *et al.* discovered suppressed phase segregation after applying PMMA on the $CsPbI_{3-x}Br_x$ microplatelet, which is attributed to the passivation of vacancies at the perovskite surface [120]. Figure 6(f) shows the PL spectra of the perovskite platelet with and without PMMA under 12 min light illumination. Later, Yang *et al.* observed a suppressed PL shift in all-inorganic $CsPbI_{3-x}Br_x$ NCs treated by KBr as the passivation agent [Fig. 6(g)], while the pristine counterpart exhibits phase segregation with the PL peak shifting from 638 nm to 661 nm [Fig. 6(h)] [115].

Other factors, such as atmosphere and light intensity, also play important roles in mitigating the halide segregation process. It has been reported that the oxygen molecules can react with photogenerated charge carriers to form superoxide species (O_2^-) [126]. The O_2^- is well suited to occupy the halide vacancies and passivate the trap states, thus influencing the phase-segregation phenomenon. Knight *et al.* have studied the correlation of an environmental atmosphere with phase segregation and its reversibility [107]. According to their report, repeated cycles of illumination and darkness yield results similar to the scenario of exposing the perovskite film to vacuum and ambient air. But the halide segregation was discovered mostly reversible when the film was exposed in a nitrogen atmosphere or encapsulated by PMMA. Fortunately, the influence of the atmosphere on the optical properties of the perovskite layer can be mitigated by the implementation of an encapsulation layer such as PMMA [107]. Moreover, phase segregation was also reported to be weakened with the reduction of light illumination intensities [48,51,52,107,127]. The reduced excited charger carriers at lower excitation intensity are responsible for the suppressed phase segregation since the photogenerated carrier is directly linked to the halide segregation according to the polaron model.

4. CONCLUSION AND OUTLOOK

All-inorganic mixed-halide perovskites are prominent candidates for advancing efficient optoelectronic devices such as solar cells and LEDs owing to their better stability compared to their hybrid counterparts and promising optical properties. However, the phase instability of perovskite materials under harsh operation environments remains a critical issue that should be addressed before the commercialization of perovskite-based technologies, and the halide segregation is emerging as another showstopper since mixing halides is prevalent in perovskite research. Although the general phase segregation phenomenon is well documented, and some mechanisms were proposed and reviewed herein, additional works are urgently needed to address some open questions. For example, as the phase-segregation process is sensitive to the film morphology and grain size, can a synthesis and processing strategy be developed as an effective mitigation method? For example, two-step spin coating, which generally yields better film qualities, may help tailor a solution-processing approach to producing segregation-free perovskite films. Furthermore, regarding the phenomena, does a critical excitation intensity exist as the threshold to induce phase segregation, and how is the value correlated with the material processing? If the excessive photogenerated carriers are directly responsible for the phase-segregation process, will doping the mixed-halide perovskite affect the optical behaviors and phase segregation under illumination? In terms of mechanisms, is the polaron-induced lattice strain the dominant factor triggering the phase segregation? Presumably, the characteristics of polarons in perovskite films can be tailored through tuning the processing conditions. When it comes to the influence of phase segregation on photovoltaic performance, the mechanistic descriptions of the phase-segregation-dependent parameters of solar cells remain elusive. Seeking answers to these open questions will be a challenging adventure as a result of the strong processing-property correlation in halide perovskites that nevertheless must be undertaken in order to achieve reliable device performance. In this review, we summarized the experimental results, mechanisms, and different mitigation strategies related to phase segregation in inorganic perovskite, which aims to give a coherent picture of this emerging field and to propose potential steps forward. For inorganic mixed-halide perovskites to be considered as the frontrunner for perovskite-based light-harvesting devices, a more comprehensive understanding of the phase-segregation phenomena is essential for the experimental design and realization of stable radiation-hard device technologies.

Funding. Australian Research Council (DP190103316); UNSW SHARP Project (RG163043); US Office of Naval Research (N00014-18-1-2408); US National Science Foundation (CMMI-1930809).

Disclosures. The authors declare no conflicts of interest.

REFERENCES

1. W. S. Yang, B.-W. Park, E. H. Jung, N. J. Jeon, Y. C. Kim, D. U. Lee, S. S. Shin, J. Seo, E. K. Kim, and J. H. Noh, "Iodide management in formamidinium-lead-halide-based perovskite layers for efficient solar cells," Science **356**, 1376–1379 (2017).
2. A. Kojima, K. Teshima, Y. Shirai, and T. Miyasaka, "Organometal halide perovskites as visible-light sensitizers for photovoltaic cells," J. Am. Chem. Soc. **131**, 6050–6051 (2009).
3. H.-S. Kim, C.-R. Lee, J.-H. Im, K.-B. Lee, T. Moehl, A. Marchioro, S.-J. Moon, R. Humphry-Baker, J.-H. Yum, and J. E. Moser, "Lead iodide perovskite sensitized all-solid-state submicron thin film mesoscopic solar cell with efficiency exceeding 9%," Sci. Rep. **2**, 591 (2012).

4. H. Zhou, Q. Chen, G. Li, S. Luo, T.-B. Song, H.-S. Duan, Z. Hong, J. You, Y. Liu, and Y. Yang, "Interface engineering of highly efficient perovskite solar cells," Science **345**, 542–546 (2014).
5. Y. Fu, F. Meng, M. B. Rowley, B. J. Thompson, M. J. Shearer, D. Ma, R. J. Hamers, J. C. Wright, and S. Jin, "Solution growth of single crystal methylammonium lead halide perovskite nanostructures for optoelectronic and photovoltaic applications," J. Am. Chem. Soc. **137**, 5810–5818 (2015).
6. Z. Chen, B. Turedi, A. Y. Alsalloum, C. Yang, X. Zheng, I. Gereige, A. AlSaggaf, O. F. Mohammed, and O. M. Bakr, "Single-crystal $MAPbI_3$ perovskite solar cells exceeding 21% power conversion efficiency," ACS Energy Lett. **4**, 1258–1259 (2019).
7. W. Peng, L. Wang, B. Murali, K.-T. Ho, A. Bera, N. Cho, C.-F. Kang, V. M. Burlakov, J. Pan, L. Sinatra, C. Ma, W. Xu, D. Shi, E. Alarousu, A. Goriely, J.-H. He, O. F. Mohammed, T. Wu, and O. M. Bakr, "Solution-grown monocrystalline hybrid perovskite films for hole-transporter-free solar cells," Adv. Mater. **28**, 3383–3390 (2016).
8. H. Zhu, Y. Fu, F. Meng, X. Wu, Z. Gong, Q. Ding, M. V. Gustafsson, M. T. Trinh, S. Jin, and X. Y. Zhu, "Lead halide perovskite nanowire lasers with low lasing thresholds and high quality factors," Nat. Mater. **14**, 636–642 (2015).
9. T. J. S. Evans, A. Schlaus, Y. Fu, X. Zhong, T. L. Atallah, M. S. Spencer, L. E. Brus, S. Jin, and X.-Y. Zhu, "Continuous-wave lasing in cesium lead bromide perovskite nanowires," Adv. Opt. Mater. **6**, 1700982 (2018).
10. Y. Mi, Y. Zhong, Q. Zhang, and X. Liu, "Continuous-wave pumped perovskite lasers," Adv. Opt. Mater. **7**, 1900544 (2019).
11. C.-H. Lin, T.-Y. Li, J. Zhang, Z.-Y. Chiao, P.-C. Wei, H.-C. Fu, L. Hu, M.-J. Yu, G. H. Ahmed, X. Guan, C.-H. Ho, T. Wu, B. S. Ooi, O. F. Mohammed, Y.-J. Lu, X. Fang, and J.-H. He, "Designed growth and patterning of perovskite nanowires for lasing and wide color gamut phosphors with long-term stability," Nano Energy **73**, 104801 (2020).
12. Z.-K. Tan, R. S. Moghaddam, M. L. Lai, P. Docampo, R. Higler, F. Deschler, M. Price, A. Sadhanala, L. M. Pazos, and D. Credgington, "Bright light-emitting diodes based on organometal halide perovskite," Nat. Nanotechnol. **9**, 687–692 (2014).
13. H. Cho, S.-H. Jeong, M.-H. Park, Y.-H. Kim, C. Wolf, C.-L. Lee, J. H. Heo, A. Sadhanala, N. Myoung, and S. J. S. Yoo, "Overcoming the electroluminescence efficiency limitations of perovskite light-emitting diodes," Science **350**, 1222–1225 (2015).
14. Y. Ling, Y. Tian, X. Wang, J. C. Wang, J. M. Knox, F. Perez-Orive, Y. Du, L. Tan, K. Hanson, and B. Ma, "Enhanced optical and electrical properties of polymer-assisted all-inorganic perovskites for light-emitting diodes," Adv. Mater. **28**, 8983–8989 (2016).
15. J. Song, J. Li, X. Li, L. Xu, Y. Dong, and H. Zeng, "Quantum dot light-emitting diodes based on inorganic perovskite cesium lead halides ($CsPbX_3$)," Adv. Mater. **27**, 7162–7167 (2015).
16. Z. Xiao, L. Zhao, N. L. Tran, Y. L. Lin, S. H. Silver, R. A. Kerner, N. Yao, A. Kahn, G. D. Scholes, and B. P. Rand, "Mixed-halide perovskites with stabilized bandgaps," Nano Lett. **17**, 6863–6869 (2017).
17. F. Li, C. Ma, H. Wang, W. Hu, W. Yu, A. D. Sheikh, and T. Wu, "Ambipolar solution-processed hybrid perovskite phototransistors," Nat. Commun. **6**, 8238 (2015).
18. K. Domanski, W. Tress, T. Moehl, M. Saliba, M. K. Nazeeruddin, and M. Grätzel, "Working principles of perovskite photodetectors: analyzing the interplay between photoconductivity and voltage-driven energy-level alignment," Adv. Funct. Mater. **25**, 6936–6947 (2015).
19. X. Liu, D. Yu, F. Cao, X. Li, J. Ji, J. Chen, X. Song, and H. Zeng, "Low-voltage photodetectors with high responsivity based on solution-processed micrometer-scale all-inorganic perovskite nanoplatelets," Small **13**, 1700364 (2017).
20. M. Ahmadi, T. Wu, and B. Hu, "A review on organic-inorganic halide perovskite photodetectors: device engineering and fundamental physics," Adv. Mater. **29**, 1605242 (2017).
21. J. Miao and F. Zhang, "Recent progress on highly sensitive perovskite photodetectors," J. Mater. Chem. C **7**, 1741–1791 (2019).
22. X. Fu, S. Jiao, Y. Jiang, L. Li, X. Wang, C. Zhu, C. Ma, H. Zhao, Z. Xu, Y. Liu, W. Huang, W. Zheng, P. Fan, F. Jiang, D. Zhang, X. Zhu, X. Wang, and A. Pan, "Large-scale growth of ultrathin low-dimensional perovskite nanosheets for high-detectivity photodetectors," ACS Appl. Mater. Interfaces **12**, 2884–2891 (2020).
23. Y. Chen, J. Zhang, J. Zhou, Y. Chu, B. Zhou, X. Wu, and J. Huang, "Long-term stable and tunable high-performance photodetectors based on perovskite microwires," Adv. Opt. Mater. **6**, 1800469 (2018).
24. X. Guan, Z. Wang, M. K. Hota, H. N. Alshareef, and T. Wu, "P-type SnO thin film phototransistor with perovskite-mediated photogating," Adv. Electron. Mater. **5**, 1800538 (2019).
25. X. Guan, Y. Wang, C.-H. Lin, L. Hu, S. Ge, T. Wan, A. Younis, F. Li, Y. Cui, D.-C. Qi, D. Chu, X. D. Chen, and T. Wu, "A monolithic artificial iconic memory based on highly stable perovskite-metal multilayers," Appl. Phys. Rev. **7**, 031401 (2020).
26. Q. Dong, Y. Fang, Y. Shao, P. Mulligan, J. Qiu, L. Cao, and J. Huang, "Electron-hole diffusion lengths >175 μm in solution-grown $CH_3NH_3PbI_3$ single crystals," Science **347**, 967–970 (2015).
27. S. D. Stranks, G. E. Eperon, G. Grancini, C. Menelaou, M. J. Alcocer, T. Leijtens, L. M. Herz, A. Petrozza, and H. J. Snaith, "Electron-hole diffusion lengths exceeding 1 micrometer in an organometal trihalide perovskite absorber," Science **342**, 341–344 (2013).
28. D. Shi, V. Adinolfi, R. Comin, M. Yuan, E. Alarousu, A. Buin, Y. Chen, S. Hoogland, A. Rothenberger, K. Katsiev, Y. Losovyj, X. Zhang, P. A. Dowben, O. F. Mohammed, E. H. Sargent, and O. M. Bakr, "Low trap-state density and long carrier diffusion in organolead trihalide perovskite single crystals," Science **347**, 519–522 (2015).
29. D. W. DeQuilettes, S. Koch, S. Burke, R. K. Paranji, A. J. Shropshire, M. E. Ziffer, and D. S. Ginger, "Photoluminescence lifetimes exceeding 8 μs and quantum yields exceeding 30% in hybrid perovskite thin films by ligand passivation," ACS Energy Lett. **1**, 438–444 (2016).
30. K. X. Steirer, P. Schulz, G. Teeter, V. Stevanovic, M. Yang, K. Zhu, and J. J. Berry, "Defect tolerance in methylammonium lead triiodide perovskite," ACS Energy Lett. **1**, 360–366 (2016).
31. B. A. Rosales, M. P. Hanrahan, B. W. Boote, A. J. Rossini, E. A. Smith, and J. Vela, "Lead halide perovskites: challenges and opportunities in advanced synthesis and spectroscopy," ACS Energy Lett. **2**, 906–914 (2017).
32. T. Yang, X. Wang, B. Zheng, Z. Qi, C. Ma, Y. Fu, Y. Fu, M. P. Hautzinger, Y. Jiang, Z. Li, P. Fan, F. Li, W. Zheng, Z. Luo, J. Liu, B. Yang, S. Chen, D. Li, L. Zhang, S. Jin, and A. Pan, "Ultrahigh-performance optoelectronics demonstrated in ultrathin perovskite-based vertical semiconductor heterostructures," ACS Nano **13**, 7996–8003 (2019).
33. Y. Chen, Y. Lei, Y. Li, Y. Yu, J. Cai, M.-H. Chiu, R. Rao, Y. Gu, C. Wang, W. Choi, H. Hu, C. Wang, Y. Li, J. Song, J. Zhang, B. Qi, M. Lin, Z. Zhang, A. E. Islam, B. Maruyama, S. Dayeh, L.-J. Li, K. Yang, Y.-H. Lo, and S. Xu, "Strain engineering and epitaxial stabilization of halide perovskites," Nature **577**, 209–215 (2020).
34. "Best research-cell efficiency chart," https://www.nrel.gov/pv/cell-efficiency.html.
35. P. Du, L. Gao, and J. Tang, "Focus on performance of perovskite light-emitting diodes," Front. Optoelectron. **13**, 235–245 (2020).
36. M. M. Lee, J. Teuscher, T. Miyasaka, T. N. Murakami, and H. J. Snaith, "Efficient hybrid solar cells based on meso-superstructured organometal halide perovskites," Science **338**, 643–647 (2012).
37. W. Travis, E. N. K. Glover, H. Bronstein, D. O. Scanlon, and R. G. Palgrave, "On the application of the tolerance factor to inorganic and hybrid halide perovskites: a revised system," Chem. Sci. **7**, 4548–4556 (2016).
38. Y. Zhou, J. Chen, O. M. Bakr, and H.-T. Sun, "Metal-doped lead halide perovskites: synthesis, properties, and optoelectronic applications," Chem. Mater. **30**, 6589–6613 (2018).
39. S.-T. Ha, R. Su, J. Xing, Q. Zhang, and Q. Xiong, "Metal halide perovskite nanomaterials: synthesis and applications," Chem. Sci. **8**, 2522–2536 (2017).
40. L. Protesescu, S. Yakunin, M. I. Bodnarchuk, F. Krieg, R. Caputo, C. H. Hendon, R. X. Yang, A. Walsh, and M. V. Kovalenko, "Nanocrystals of cesium lead halide perovskites ($CsPbX_3$, X= Cl, Br, and I): novel optoelectronic materials showing bright emission with wide color gamut," Nano Lett. **15**, 3692–3696 (2015).
41. D. Zhang, Y. Yang, Y. Bekenstein, Y. Yu, N. A. Gibson, A. B. Wong, S. W. Eaton, N. Kornienko, Q. Kong, and M. Lai, "Synthesis of composition tunable and highly luminescent cesium lead halide

nanowires through anion-exchange reactions," J. Am. Chem. Soc. **138**, 7236–7239 (2016).
42. C. K. Siu, J. Zhao, Y. Wang, D. Yang, X. Xu, S. Pan, and S. F. Yu, "Lasing characteristics of single-crystalline $CsPbCl_3$ perovskite microcavities under multiphoton excitation," J. Phys. D **50**, 225101 (2017).
43. Y. Zhou and Y. Zhao, "Chemical stability and instability of inorganic halide perovskites," Energy Environ. Sci. **12**, 1495–1511 (2019).
44. A. J. Knight and L. M. Herz, "Preventing phase segregation in mixed-halide perovskites: a perspective," Energy Environ. Sci. **13**, 2024–2046 (2020).
45. A. Marronnier, G. Roma, S. Boyer-Richard, L. Pedesseau, J.-M. Jancu, Y. Bonnassieux, C. Katan, C. C. Stoumpos, M. G. Kanatzidis, and J. Even, "Anharmonicity and disorder in the black phases of cesium lead iodide used for stable inorganic perovskite solar cells," ACS Nano **12**, 3477–3486 (2018).
46. J. A. Steele, H. Jin, I. Dovgaliuk, R. F. Berger, T. Braeckevelt, H. Yuan, C. Martin, E. Solano, K. Lejaeghere, S. M. J. Rogge, C. Notebaert, W. Vandezande, K. P. F. Janssen, B. Goderis, E. Debroye, Y.-K. Wang, Y. Dong, D. Ma, M. Saidaminov, H. Tan, Z. Lu, V. Dyadkin, D. Chernyshov, V. Van Speybroeck, E. H. Sargent, J. Hofkens, and M. B. J. Roeffaers, "Thermal unequilibrium of strained black $CsPbI_3$ thin films," Science **365**, 679–684 (2019).
47. Z. Cheng and J. Lin, "Layered organic-inorganic hybrid perovskites: structure, optical properties, film preparation, patterning and templating engineering," CrystEngComm **12**, 2646–2662 (2010).
48. E. T. Hoke, D. J. Slotcavage, E. R. Dohner, A. R. Bowring, H. I. Karunadasa, and M. D. McGehee, "Reversible photo-induced trap formation in mixed-halide hybrid perovskites for photovoltaics," Chem. Sci. **6**, 613–617 (2015).
49. D. J. Slotcavage, H. I. Karunadasa, and M. D. McGehee, "Light-induced phase segregation in halide-perovskite absorbers," ACS Energy Lett. **1**, 1199–1205 (2016).
50. C. G. Bischak, C. L. Hetherington, H. Wu, S. Aloni, D. F. Ogletree, D. T. Limmer, and N. S. Ginsberg, "Origin of reversible photoinduced phase separation in hybrid perovskites," Nano Lett. **17**, 1028–1033 (2017).
51. S. J. Yoon, S. Draguta, J. S. Manser, O. Sharia, W. F. Schneider, M. Kuno, and P. V. Kamat, "Tracking iodide and bromide ion segregation in mixed halide lead perovskites during photoirradiation," ACS Energy Lett. **1**, 290–296 (2016).
52. S. Draguta, O. Sharia, S. J. Yoon, M. C. Brennan, Y. V. Morozov, J. S. Manser, P. V. Kamat, W. F. Schneider, and M. Kuno, "Rationalizing the light-induced phase separation of mixed halide organic-inorganic perovskites," Nat. Commun. **8**, 200 (2017).
53. Z. Yang, A. Rajagopal, S. B. Jo, C.-C. Chueh, S. Williams, C.-C. Huang, J. K. Katahara, H. W. Hillhouse, and A. K. Y. Jen, "Stabilized wide bandgap perovskite solar cells by tin substitution," Nano Lett. **16**, 7739–7747 (2016).
54. A. J. Barker, A. Sadhanala, F. Deschler, M. Gandini, S. P. Senanayak, P. M. Pearce, E. Mosconi, A. J. Pearson, Y. Wu, A. R. Srimath Kandada, T. Leijtens, F. De Angelis, S. E. Dutton, A. Petrozza, and R. H. Friend, "Defect-assisted photoinduced halide segregation in mixed-halide perovskite thin films," ACS Energy Lett. **2**, 1416–1424 (2017).
55. S. J. Yoon, M. Kuno, and P. V. Kamat, "Shift happens. How halide ion defects influence photoinduced segregation in mixed halide perovskites," ACS Energy Lett. **2**, 1507–1514 (2017).
56. I. L. Braly, R. J. Stoddard, A. Rajagopal, A. R. Uhl, J. K. Katahara, A. K. Y. Jen, and H. W. Hillhouse, "Current-induced phase segregation in mixed halide hybrid perovskites and its impact on two-terminal tandem solar cell design," ACS Energy Lett. **2**, 1841–1847 (2017).
57. M. Hu, C. Bi, Y. Yuan, Y. Bai, and J. Huang, "Stabilized wide bandgap $MAPbBr_xI_{3-x}$ perovskite by enhanced grain size and improved crystallinity," Adv. Sci. **3**, 1500301 (2016).
58. W. Li, M. U. Rothmann, A. Liu, Z. Wang, Y. Zhang, A. R. Pascoe, J. Lu, L. Jiang, Y. Chen, F. Huang, Y. Peng, Q. Bao, J. Etheridge, U. Bach, and Y.-B. Cheng, "Phase segregation enhanced ion movement in efficient inorganic $CsPbIBr_2$ solar cells," Adv. Energy Mater. **7**, 1700946 (2017).
59. F. Brivio, C. Caetano, and A. Walsh, "Thermodynamic origin of photoinstability in the $CH_3NH_3Pb(I_{1-x}Br_x)_3$ hybrid halide perovskite alloy," J. Phys. Chem. Lett. **7**, 1083–1087 (2016).
60. U. B. Cappel, S. Svanström, V. Lanzilotto, F. O. L. Johansson, K. Aitola, B. Philippe, E. Giangrisostomi, R. Ovsyannikov, T. Leitner, A. Föhlisch, S. Svensson, N. Mårtensson, G. Boschloo, A. Lindblad, and H. Rensmo, "Partially reversible photoinduced chemical changes in a mixed-ion perovskite material for solar cells," ACS Appl. Mater. Interfaces **9**, 34970–34978 (2017).
61. X. Wang, Y. Ling, X. Lian, Y. Xin, K. B. Dhungana, F. Perez-Orive, J. Knox, Z. Chen, Y. Zhou, D. Beery, K. Hanson, J. Shi, S. Lin, and H. Gao, "Suppressed phase separation of mixed-halide perovskites confined in endotaxial matrices," Nat. Commun. **10**, 695 (2019).
62. H. Zhang, X. Fu, Y. Tang, H. Wang, C. Zhang, W. Y. William, X. Wang, Y. Zhang, and M. Xiao, "Phase segregation due to ion migration in all-inorganic mixed-halide perovskite nanocrystals," Nat. Commun. **10**, 1088 (2019).
63. A. F. Gualdrón-Reyes, S. J. Yoon, E. M. Barea, S. Agouram, V. Muñoz-Sanjosé, Á. M. Meléndez, M. E. Niño-Gómez, and I. Mora-Seró, "Controlling the phase segregation in mixed halide perovskites through nanocrystal size," ACS Energy Lett. **4**, 54–62 (2019).
64. M. C. Brennan, S. Draguta, P. V. Kamat, and M. Kuno, "Light-induced anion phase segregation in mixed halide perovskites," ACS Energy Lett. **3**, 204–213 (2017).
65. W. Zhou, Y. Zhao, X. Zhou, R. Fu, Q. Li, Y. Zhao, K. Liu, D. Yu, and Q. Zhao, "Light-independent ionic transport in inorganic perovskite and ultrastable Cs-based perovskite solar cells," J. Phys. Chem. Lett. **8**, 4122–4128 (2017).
66. M. C. Brennan, A. Ruth, P. V. Kamat, and M. Kuno, "Photoinduced anion segregation in mixed halide perovskites," Trends Chem. **2**, 282–301 (2020).
67. G. F. Samu, C. Janáky, and P. V. Kamat, "A victim of halide ion segregation. How light soaking affects solar cell performance of mixed halide lead perovskites," ACS Energy Lett. **2**, 1860–1861 (2017).
68. J. Hu, R. Gottesman, L. Gouda, A. Kama, M. Priel, S. Tirosh, J. Bisquert, and A. Zaban, "Photovoltage behavior in perovskite solar cells under light-soaking showing photoinduced interfacial changes," ACS Energy Lett. **2**, 950–956 (2017).
69. R. J. Sutton, G. E. Eperon, L. Miranda, E. S. Parrott, B. A. Kamino, J. B. Patel, M. T. Hörantner, M. B. Johnston, A. A. Haghighirad, D. T. Moore, and H. J. Snaith, "Bandgap-tunable cesium lead halide perovskites with high thermal stability for efficient solar cells," Adv. Energy Mater. **6**, 1502458 (2016).
70. J. K. Nam, M. S. Jung, S. U. Chai, Y. J. Choi, D. Kim, and J. H. Park, "Unveiling the crystal formation of cesium lead mixed-halide perovskites for efficient and stable solar cells," J. Phys. Chem. Lett. **8**, 2936–2940 (2017).
71. J. Burschka, N. Pellet, S.-J. Moon, R. Humphry-Baker, P. Gao, M. K. Nazeeruddin, and M. Grätzel, "Sequential deposition as a route to high-performance perovskite-sensitized solar cells," Nature **499**, 316–319 (2013).
72. A. R. Pascoe, Q. Gu, M. U. Rothmann, W. Li, Y. Zhang, A. D. Scully, X. Lin, L. Spiccia, U. Bach, and Y.-B. Cheng, "Directing nucleation and growth kinetics in solution-processed hybrid perovskite thin-films," Sci. China Mater. **60**, 617–628 (2017).
73. S. J. Yoon, K. G. Stamplecoskie, and P. V. Kamat, "How lead halide complex chemistry dictates the composition of mixed halide perovskites," J. Phys. Chem. Lett. **7**, 1368–1373 (2016).
74. J.-H. Im, H.-S. Kim, and N.-G. Park, "Morphology-photovoltaic property correlation in perovskite solar cells: one-step versus two-step deposition of $CH_3NH_3PbI_3$," APL Mater. **2**, 081510 (2014).
75. N. J. Jeon, J. H. Noh, Y. C. Kim, W. S. Yang, S. Ryu, and S. I. Seok, "Solvent engineering for high-performance inorganic-organic hybrid perovskite solar cells," Nat. Mater. **13**, 897–903 (2014).
76. S. Lou, T. Xuan, Q. Liang, J. Huang, L. Cao, C. Yu, M. Cao, C. Xia, J. Wang, D. Zhang, and H. Li, "Controllable and facile synthesis of $CsPbBr_3$-Cs_4PbBr_6 perovskite composites in pure polar solvent," J. Colloid Interface Sci. **537**, 384–388 (2019).

77. H. Gaonkar, J. Zhu, R. Kottokkaran, B. Bhageri, M. Noack, and V. Dalal, "Thermally stable, efficient, vapor deposited inorganic perovskite solar cells," ACS Appl. Energy Mater. **3**, 3497–3503 (2020).
78. Q. Ma, S. Huang, X. Wen, M. A. Green, and A. W. Y. Ho-Baillie, "Hole transport layer free inorganic $CsPbIBr_2$ perovskite solar cell by dual source thermal evaporation," Adv. Energy Mater. **6**, 1502202 (2016).
79. C.-Y. Chen, H.-Y. Lin, K.-M. Chiang, W.-L. Tsai, Y.-C. Huang, C.-S. Tsao, and H.-W. Lin, "All-vacuum-deposited stoichiometrically balanced inorganic cesium lead halide perovskite solar cells with stabilized efficiency exceeding 11%," Adv. Mater. **29**, 1605290 (2017).
80. Q. Zeng, X. Zhang, X. Feng, S. Lu, Z. Chen, X. Yong, S. A. T. Redfern, H. Wei, H. Wang, H. Shen, W. Zhang, W. Zheng, H. Zhang, J. S. Tse, and B. Yang, "Polymer-passivated inorganic cesium lead mixed-halide perovskites for stable and efficient solar cells with high open-circuit voltage over 1.3 V," Adv. Mater. **30**, 1705393 (2018).
81. M. De Bastiani, V. D'Innocenzo, S. D. Stranks, H. J. Snaith, and A. Petrozza, "Role of the crystallization substrate on the photoluminescence properties of organo-lead mixed halides perovskites," APL Mater. **2**, 081509 (2014).
82. W. Qiu, T. Merckx, M. Jaysankar, C. M. de la Huerta, L. Rakocevic, W. Zhang, U. W. Paetzold, R. Gehlhaar, L. Froyen, J. Poortmans, D. Cheyns, H. J. Snaith, and P. Heremans, "Pinhole-free perovskite films for efficient solar modules," Energy Environ. Sci. **9**, 484–489 (2016).
83. M. R. Ahmadian-Yazdi, F. Zabihi, M. Habibi, and M. Eslamian, "Effects of process parameters on the characteristics of mixed-halide perovskite solar cells fabricated by one-step and two-step sequential coating," Nanoscale Res. Lett. **11**, 408 (2016).
84. D. Chen, S. Yuan, J. Chen, J. Zhong, and X. Xu, "Robust $CsPbX_3$ (X = Cl, Br, and I) perovskite quantum dot embedded glasses: nanocrystallization, improved stability and visible full-spectral tunable emissions," J. Mater. Chem. C **6**, 12864–12870 (2018).
85. W. Shockley and H. J. Queisser, "Detailed balance limit of efficiency of p-n junction solar cells," J. Appl. Phys. **32**, 510–519 (1961).
86. G. R. Berdiyorov, A. Kachmar, F. El-Mellouhi, M. A. Carignano, and M. E. Madjet, "Role of cations on the electronic transport and optical properties of lead-iodide perovskites," J. Phys. Chem. C **120**, 16259–16270 (2016).
87. Z. Yang, A. Surrente, K. Galkowski, A. Miyata, O. Portugall, R. J. Sutton, A. A. Haghighirad, H. J. Snaith, D. K. Maude, P. Plochocka, and R. J. Nicholas, "Impact of the halide cage on the electronic properties of fully inorganic cesium lead halide perovskites," ACS Energy Lett. **2**, 1621–1627 (2017).
88. X. Li, Y. Wu, S. Zhang, B. Cai, Y. Gu, J. Song, and H. Zeng, "$CsPbX_3$ quantum dots for lighting and displays: room-temperature synthesis, photoluminescence superiorities, underlying origins and white light-emitting diodes," Adv. Funct. Mater. **26**, 2435–2445 (2016).
89. B. Zhao, S.-F. Jin, S. Huang, N. Liu, J.-Y. Ma, D.-J. Xue, Q. Han, J. Ding, Q.-Q. Ge, Y. Feng, and J.-S. Hu, "Thermodynamically stable orthorhombic γ-$CsPbI_3$ thin films for high-performance photovoltaics," J. Am. Chem. Soc. **140**, 11716–11725 (2018).
90. Y. Wang, M. I. Dar, L. K. Ono, T. Zhang, M. Kan, Y. Li, L. Zhang, X. Wang, Y. Yang, X. Gao, Y. Qi, M. Grätzel, and Y. Zhao, "Thermodynamically stabilized β-$CsPbI_3$-based perovskite solar cells with efficiencies >18%," Science **365**, 591–595 (2019).
91. Z. Qiu, N. Li, Z. Huang, Q. Chen, and H. Zhou, "Recent advances in improving phase stability of perovskite solar cells," Small Methods **4**, 1900877 (2020).
92. Z. Li, F. Zhou, Q. Wang, L. Ding, and Z. Jin, "Approaches for thermodynamically stabilized $CsPbI_3$ solar cells," Nano Energy **71**, 104634 (2020).
93. Y. Wang, X. Guan, D. Li, H.-C. Cheng, X. Duan, Z. Lin, and X. Duan, "Chemical vapor deposition growth of single-crystalline cesium lead halide microplatelets and heterostructures for optoelectronic applications," Nano Res. **10**, 1223–1233 (2017).
94. N. N. Lal, T. P. White, and K. R. Catchpole, "Optics and light trapping for tandem solar cells on silicon," IEEE J. Photovoltaics **4**, 1380–1386 (2014).
95. X. Li, F. Cao, D. Yu, J. Chen, Z. Sun, Y. Shen, Y. Zhu, L. Wang, Y. Wei, Y. Wu, and H. Zeng, "All inorganic halide perovskites nanosystem: synthesis, structural features, optical properties and optoelectronic applications," Small **13**, 1603996 (2017).
96. T. Markvart, "Semiclassical theory of non-radiative transitions," J. Phys. C **14**, L895–L899 (1981).
97. A. Marronnier, G. Roma, M. A. Carignano, Y. Bonnassieux, C. Katan, J. Even, E. Mosconi, and F. De Angelis, "Influence of disorder and anharmonic fluctuations on the dynamical rashba effect in purely inorganic lead-halide perovskites," J. Phys. Chem. C **123**, 291–298 (2019).
98. Q. Van Le, M. Park, W. Sohn, H. W. Jang, and S. Y. Kim, "Investigation of energy levels and crystal structures of cesium lead halides and their application in full-color light-emitting diodes," Adv. Electron. Mater. **3**, 1600448 (2017).
99. J. A. Sichert, Y. Tong, N. Mutz, M. Vollmer, S. Fischer, K. Z. Milowska, R. García Cortadella, B. Nickel, C. Cardenas-Daw, J. K. Stolarczyk, A. S. Urban, and J. Feldmann, "Quantum size effect in organometal halide perovskite nanoplatelets," Nano Lett. **15**, 6521–6527 (2015).
100. R. E. Beal, D. J. Slotcavage, T. Leijtens, A. R. Bowring, R. A. Belisle, W. H. Nguyen, G. F. Burkhard, E. T. Hoke, and M. D. McGehee, "Cesium lead halide perovskites with improved stability for tandem solar cells," J. Phys. Chem. Lett. **7**, 746–751 (2016).
101. D. P. Norton, "Synthesis and properties of epitaxial electronic oxide thin-film materials," Mater. Sci. Eng. R **43**, 139–247 (2004).
102. W. Chen, W. Mao, U. Bach, B. Jia, and X. Wen, "Tracking dynamic phase segregation in mixed-halide perovskite single crystals under two-photon scanning laser illumination," Small Methods **3**, 1900273 (2019).
103. W. Chen, W. Li, Z. Gan, Y.-B. Cheng, B. Jia, and X. Wen, "Long-distance ionic diffusion in cesium lead mixed halide perovskite induced by focused illumination," Chem. Mater. **31**, 9049–9056 (2019).
104. T. Duong, H. K. Mulmudi, Y. Wu, X. Fu, H. Shen, J. Peng, N. Wu, H. T. Nguyen, D. Macdonald, M. Lockrey, T. P. White, K. Weber, and K. Catchpole, "Light and electrically induced phase segregation and its impact on the stability of quadruple cation high bandgap perovskite solar cells," ACS Appl. Mater. Interfaces **9**, 26859–26866 (2017).
105. N. Li, Z. Zhu, J. Li, A. K.-Y. Jen, and L. Wang, "Inorganic $CsPb_{1-x}Sn_xIBr_2$ for efficient wide-bandgap perovskite solar cells," Adv. Energy Mater. **8**, 1800525 (2018).
106. C. G. Bischak, A. B. Wong, E. Lin, D. T. Limmer, P. Yang, and N. S. Ginsberg, "Tunable polaron distortions control the extent of halide demixing in lead halide perovskites," J. Phys. Chem. Lett. **9**, 3998–4005 (2018).
107. A. J. Knight, A. D. Wright, J. B. Patel, D. P. McMeekin, H. J. Snaith, M. B. Johnston, and L. M. Herz, "Electronic traps and phase segregation in lead mixed-halide perovskite," ACS Energy Lett. **4**, 75–84 (2019).
108. R. A. Belisle, K. A. Bush, L. Bertoluzzi, A. Gold-Parker, M. F. Toney, and M. D. McGehee, "Impact of surfaces on photoinduced halide segregation in mixed-halide perovskites," ACS Energy Lett. **3**, 2694–2700 (2018).
109. J. Yang, Y. Wang, T. Wu, and S. Li, "Correlating the compositional-dependent structural and electronic dynamics of inorganic mixed halide perovskites," Chem. Mater. **32**, 2470–2481 (2020).
110. A. Mattoni, A. Filippetti, and C. Caddeo, "Modeling hybrid perovskites by molecular dynamics," J. Phys. Condens. Matter **29**, 043001 (2016).
111. A. Ruth, M. C. Brennan, S. Draguta, Y. V. Morozov, M. Zhukovskyi, B. Janko, P. Zapol, and M. Kuno, "Vacancy-mediated anion photosegregation kinetics in mixed halide hybrid perovskites: coupled kinetic Monte Carlo and optical measurements," ACS Energy Lett. **3**, 2321–2328 (2018).
112. D. Guo, Z. Andaji Garmaroudi, M. Abdi-Jalebi, S. D. Stranks, and T. J. Savenije, "Reversible removal of intermixed shallow states by light soaking in multication mixed halide perovskite films," ACS Energy Lett. **4**, 2360–2367 (2019).
113. Y. Zhou, Y.-H. Jia, H.-H. Fang, M. A. Loi, F.-Y. Xie, L. Gong, M.-C. Qin, X.-H. Lu, C.-P. Wong, and N. Zhao, "Composition-tuned wide

bandgap perovskites: from grain engineering to stability and performance improvement," Adv. Funct. Mater. **28**, 1803130 (2018).
114. M. Abdi-Jalebi, Z. Andaji-Garmaroudi, S. Cacovich, C. Stavrakas, B. Philippe, J. M. Richter, M. Alsari, E. P. Booker, E. M. Hutter, A. J. Pearson, S. Lilliu, T. J. Savenije, H. Rensmo, G. Divitini, C. Ducati, R. H. Friend, and S. D. Stranks, "Maximizing and stabilizing luminescence from halide perovskites with potassium passivation," Nature **555**, 497–501 (2018).
115. J.-N. Yang, Y. Song, J.-S. Yao, K.-H. Wang, J.-J. Wang, B.-S. Zhu, M.-M. Yao, S. U. Rahman, Y.-F. Lan, F.-J. Fan, and H.-B. Yao, "Potassium bromide surface passivation on $CsPbI_{3-x}Br_x$ nanocrystals for efficient and stable pure red perovskite light-emitting diodes," J. Am. Chem. Soc. **142**, 2956–2967 (2020).
116. R. G. Balakrishna, S. M. Kobosko, and P. V. Kamat, "Mixed halide perovskite solar cells. consequence of iodide treatment on phase segregation recovery," ACS Energy Lett. **3**, 2267–2272 (2018).
117. Z. Andaji-Garmaroudi, M. Abdi-Jalebi, D. Guo, S. Macpherson, A. Sadhanala, E. M. Tennyson, E. Ruggeri, M. Anaya, K. Galkowski, R. Shivanna, K. Lohmann, K. Frohna, S. Mackowski, T. J. Savenije, R. H. Friend, and S. D. Stranks, "A highly emissive surface layer in mixed-halide multication perovskites," Adv. Mater. **31**, 1902374 (2019).
118. D. Bi, W. Tress, M. I. Dar, P. Gao, J. Luo, C. Renevier, K. Schenk, A. Abate, F. Giordano, J.-P. Correa Baena, J.-D. Decoppet, S. M. Zakeeruddin, M. K. Nazeeruddin, M. Grätzel, and A. Hagfeldt, "Efficient luminescent solar cells based on tailored mixed-cation perovskites," Sci. Adv. **2**, e1501170 (2016).
119. Y. Hu, E. M. Hutter, P. Rieder, I. Grill, J. Hanisch, M. F. Aygüler, A. G. Hufnagel, M. Handloser, T. Bein, A. Hartschuh, K. Tvingstedt, V. Dyakonov, A. Baumann, T. J. Savenije, M. L. Petrus, and P. Docampo, "Understanding the role of cesium and rubidium additives in perovskite solar cells: trap states, charge transport, and recombination," Adv. Energy Mater. **8**, 1703057 (2018).
120. Z. Wang, Y. Wang, Z. Nie, Y. Ren, and H. Zeng, "Laser induced ion migration in all-inorganic mixed halide perovskite micro-platelets," Nanoscale Adv. **1**, 4459–4465 (2019).
121. Y.-M. Xie, Z. Zeng, X. Xu, C. Ma, Y. Ma, M. Li, C.-S. Lee, and S.-W. Tsang, "FA-assistant iodide coordination in organic-inorganic wide-bandgap perovskite with mixed halides," Small **16**, 1907226 (2020).
122. H. Khassaf, S. K. Yadavalli, Y. Zhou, N. P. Padture, and A. I. Kingon, "Effect of grain boundaries on charge transport in methylammonium lead iodide perovskite thin films," J. Phys. Chem. C **123**, 5321–5325 (2019).
123. J. S. Yun, J. Seidel, J. Kim, A. M. Soufiani, S. Huang, J. Lau, N. J. Jeon, S. I. Seok, M. A. Green, and A. Ho-Baillie, "Critical role of grain boundaries for ion migration in formamidinium and methylammonium lead halide perovskite solar cells," Adv. Energy Mater. **6**, 1600330 (2016).
124. F. Zheng, W. Chen, T. Bu, K. P. Ghiggino, F. Huang, Y. Cheng, P. Tapping, T. W. Kee, B. Jia, and X. Wen, "Triggering the passivation effect of potassium doping in mixed-cation mixed-halide perovskite by light illumination," Adv. Energy Mater. **9**, 1901016 (2019).
125. J. Yuan, L. Zhang, C. Bi, M. Wang, and J. Tian, "Surface trap states passivation for high-performance inorganic perovskite solar cells," Solar RRL **2**, 1800188 (2018).
126. R. Brenes, C. Eames, V. Bulović, M. S. Islam, and S. D. Stranks, "The impact of atmosphere on the local luminescence properties of metal halide perovskite grains," Adv. Mater. **30**, 1706208 (2018).
127. T. Elmelund, B. Seger, M. Kuno, and P. V. Kamat, "How interplay between photo and thermal activation dictates halide ion segregation in mixed halide perovskites," ACS Energy Lett. **5**, 56–63 (2020).